INTERNATIONAL ATOMIC ENERGY AGENCY
UNITED NATIONS EDUCATIONAL, SCIENTIFIC AND CULTURAL ORGANIZATION

INTERNATIONAL CENTRE FOR THEORETICAL PHYSICS
34100 TRIESTE (ITALY) - P.O.B. 586 - MIRAMARE - STRADA COSTIERA 11 - TELEPHONE: 2240-1
CABLE: CENTRATOM - TELEX 460392 - I

SMR/389 - 5

# WORKING PARTY ON MODELLING THERMOMECHANICAL BEHAVIOUR OF MATERIALS (29 May - 16 June 1989)

## ELASTO-PLASTIC MODELLING OF NON CUBIC MATERIALS

C. TOME'
Universidad Nacional de Rosario
Instituto de Fisica
Bv. 27 de Febrero 210 (Bis)
2000 Rosario
Argentina

# ANALYSIS OF PLASTIC ANISOTROPY OF ROLLED ZIRCALOY-4

C. Tome

IFIR-CONICET, Av.Pellegini 250, 2000 Rosario, Argentina.

A. Pochettino

Depto. Materiales, Gcia. Desarrolllo, CNEA, Av. Libertador 8250
1429 Capital, Argentina.

R. Penelle

Lab. de Metallurgie Structurale, Bat 413, Univ. de Paris Sud
91405 Orsay, France.

## Introduction

Zircaloy-4 is a zirconium alloy used in nuclear applications which, as most hexagonal materials, exhibits a marked plastic anisotropy. Here we present the results of experimental and theoretical studies done on annealed sheets of rolled Zircaloy-4 together with a critical discussion of the role of texture and of the deformation mechanisms involved. The aim of the work is to predict the formability characteristics of the material. The three main elements of the analysis that follows are: the texture of the polycrystal, the polycrystal yield surface (PCYS) and the single crystal yield surface (SCYS).

The PCYS is the locus of all the stress states which produce plastic yielding in the polycrystal. The plastic strain associated with a given yield stress is given by the normal to the surface at that point (normality rule). The same concept holds for the SCYS, which is a faceted hypersurface in stress space. Each facet is associated with a deformation system and its distance to the origin is proportional to the critical resolved shear stress (CRSS) on that system (1).

## Experimental results

Experimental textures where determined from $(10\bar{1}0)$, (0002) and $(10\bar{1}1)$ pole figures measured by X-ray diffraction. The basal poles show a characteristic tilting of 35° away from the ND and towards the TD, with the prism poles oriented in the RD (Fig. 1a). The ODF was calculated to an order l=16 and only the even component was retained. For the theoretical calculations the crystallographic texture was represented by 980 discrete orientations, each one associated with a box in Euler space of volume $\delta\Phi\times\delta\phi\times\delta\cos\theta$ - cte . The volume fraction assigned to the corresponding orientation is given by the integral of the ODF inside each box (2). Because of the combined symmetry of the crystal and the sample only a reduced region of Euler space is required, namely $0<\Phi\leq\pi/2$ , $0<\theta\leq\pi/2$ , $0<\phi\leq\pi/3$ . Here $\Phi,\theta,\phi$ are the

Eighth International Conference on
Textures of Materials (ICOTOM 8)
Edited by J.S. Kallend and G. Gottstein
The Metallurgical Society, 1988

Euler angles according to Roe's convention. The (0002) pole figure recalculated using only 300 of the 980 orientations (70% volume fraction) is given in Fig.1b. It can be seen that the agreement with the experimental pole figure is good.

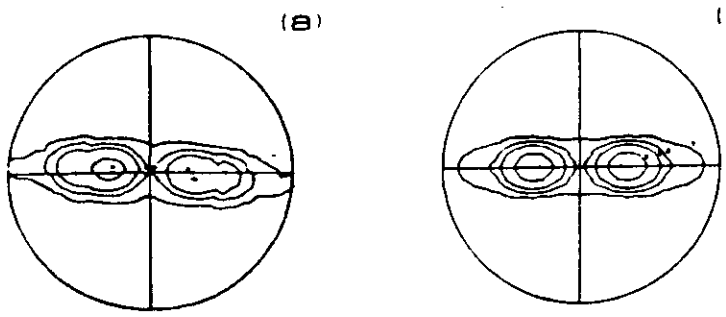


Figure 1: Normalized Zrly-4 (0002) pole figures: (a) experimental. (b) recalculated using 300 discrete orientations. Pole density levels are: 1,2,3 and 5 .

Tensile and compressive tests were performed on specimens cut from the rolled sheet. The yield stress was measured along the RD and TD in tension and along the RD, TD and ND in compression. Values of 322, 403, 370, 405 and 550 MPa were obtained respectively. The Lankford coefficient R was determined from plastic strain measurements done on tensile specimens cut from the sheet at an angle $\alpha$ with respect to the rolling direction. The result of these experiments are discussed in what follows in connection with the theoretic predictions.

## Theoretical analysis

The macroscopic plastic behavior of the polycrystal is a consequence of its texture and the plastic properties of the constituent grains. In particular, Canova et al (3) have shown that the yield stress in the polycrystal is given by the average over the stress state in each grain, weighted by the corresponding volume fraction. As a consequence, it is possible to build the PCYS by probing the polycrystal in different strain directions and averaging the resulting stresses over all the grains. Because of the orthotropic symmetry of the rolling texture the subspace $(\sigma_{11},\sigma_{22},\sigma_{33})$ formed by the diagonal deviatoric stress and strain components and the subspace $(\sigma_{11},\sigma_{22},\sigma_{33},\sigma_{12})$ are "closed" (3). That is to say: if the non zero components of the imposed strain belong to one of those subspaces, so do the resultant non zero stress components and viceversa (provided that the tensors are represented in the orthotropic axes). To construct the deviatoric plane representation of the PCYS it suffices to probe the aggregate with strains belonging to the first subspace. As for the calculation of the Lankford coefficient, except for $\alpha$=0° or $\alpha$=90°, the search has to be done within the second subspace. R results from probing the PCYS until a pure tensile stress state is found along the direction defined by $\alpha$.



Two methods were used in this work for evaluating the yield stress in the grains associated with an externally imposed deformation: a classical relaxed Taylor and a self consistent method. Within the Taylor approach the same strain is imposed onto every grain and the stress is given by the vertex of the SCYS which maximizes the plastic work. The relaxation of the strain components $\epsilon_{13}$ and $\epsilon_{23}$ is based on the flat shape of the rolled grains but does not modify the results because of the closedness of the subspace $(\sigma_{11},\sigma_{22},\sigma_{33},\sigma_{12})$. The second approach, which we regard as a more realistic representation of polycrystal plasticity, is based on a self-consistent visco-plastic calculation described in detail in references (4,5). Its main features are: it allows for different amounts of deformation from grain to grain depending on the grain's orientation, plastic anisotropy, shape and degree of hardening; it requires less than five active systems in each grain; the deviation in the stress components with respect to the mean is about half the deviation that results from applying Taylor and the deviation in the strain components is now different from zero and of the same order as the stress deviations. Results obtained using each model are presented in the next section.

## Results and discussion

The calculations that follow were done assumming that at room temperature the active systems in Zircaloy-4 are: $(10\bar{1}0)$ $<11\bar{2}0>$ prism slip, $(10\bar{1}1)$ $<11\bar{2}3>$ pyramidal slip, $(10\bar{1}2)$ $<10\bar{1}1>$ tensile twins and $(2\bar{1}\bar{1}2)$ $<2\bar{1}\bar{1}3>$ compressive twins (6). The CRSS's associated with these systems are to a large extent unknown and for the case of twinning it is not clear whether they are activated by a CRSS alone or if the stress component perpendicular to the twinnig plane also plays a role (7). In what follows the CRSS's will be normalized by the CRSS of the pyramidal systems. For the present study values of 1.0, 0.5, 0.7 and 0.8 for pyramidal, prismatic, tensile and compressive twins respectively provide the most reasonable agreement with the experimental results. Those values are also consistent with simulated rolling textures in the same material (8). Results do not change substantially if values of around 1.0 are used for the CRSS on the twinning systems.

Deviatoric plane representations of the PCYS calculated inserting the previous values into the Taylor and the self consistent models are reported in Fig.2 . A total of 300 grains, representing 70% of the polycrystal volume, was used to perform the calculation. For comparison purposes the experimental values are superimposed and the PCYS is normalized to the compressive yield stress in the normal direction. The PCYS calculated using the Taylor approach (Fig 2a) does not differ markedly from the one predicted by the self-consistent calculation (Fig 2b). The SCYS of a single grain tilted 35° with respect to the normal direction is plotted in Fig. 2c and it can be seen that it already exhibits the most prominent features of Figs 2a and 2b, namely: a counterclockwise tilting with respect to the experimental points and a positive $\epsilon_{33}$ component for the strain vector associated with tensile stress along the TD. This latter feature is linked to a singularity in the predicted Lankford coefficient.

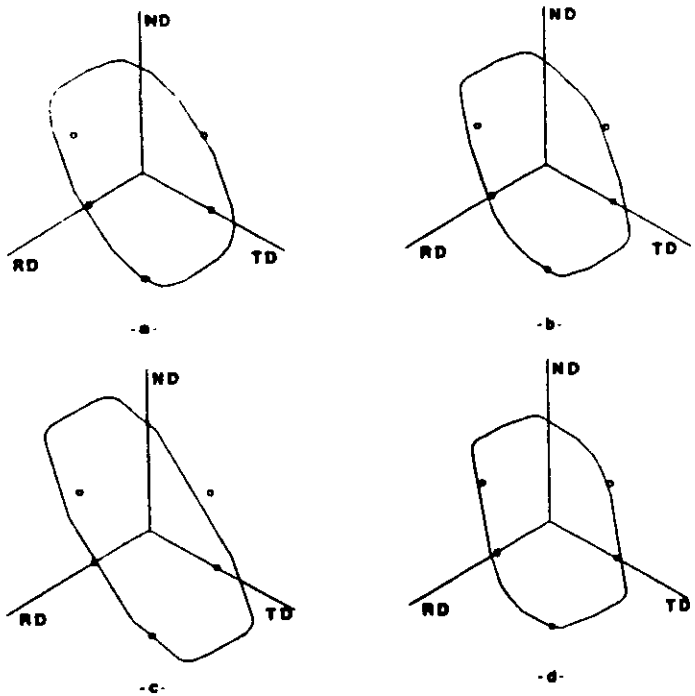


Figure 2: Predicted PCYS using (a) Relaxed Taylor model; (b) self-consistent calculation. (c) Predicted SCYS for the principal texture component. (d) PCYS for reoriented texture after tensile test along TD. The relative CRSS's used are: 1.0, 0.5, 0.7 and 0.8 for pyramidal and prism slip, tensile and compressive twins respectively.

Statistics performed on the slip and twinning activity for the Taylor case show that when the stress is along the RD prism slip amounts to about 50% of the total shear, pyramidal slip to about 30% and either compressive or tensile twins provide the remaining 20% in tension and compression respectively. Along the TD direction we predict 40% prism activity, 50% pyramidal slip and the remaining 10% is accomodated by twinning. Along the ND the pyramidal systems contribute 50% of the activity, the prismatic systems 35% and the rest comes from either type of twin depending on the sense of the stress. The main differences with the results derived using the self consistent approach are: now an average of about 3.5 systems are active as opposed to 5.5 in the Taylor calculation; there is an enhancement of the prism activity along the RD and the TD (about 80%) and a complementary decrease of the pyramidal activity. Twinning activity increases to about 50% for stress states along the ND.



As for the calculation of the Lankford coefficient the most prominent feature in Figs 2a-2c is the direction of the normal to the PCYS at the intersection with the TD: it is evident that for a tensile stress along the transverse direction the resultant strain components are such that the specimen will tend to expand along the through thickness direction, leading to a negative value of the Lankford coefficient. Predicted values of R are plotted in Fig.4 where it can be seen that the anomalous behavior starts at around 60°. The effect is more marked in the self consistent calculation because in this case the deformation tends to be accomodated mostly by prismatic slip, a fact that combined with the angle of the predominant basal poles leads naturally to an expansion in the through thickness direction.

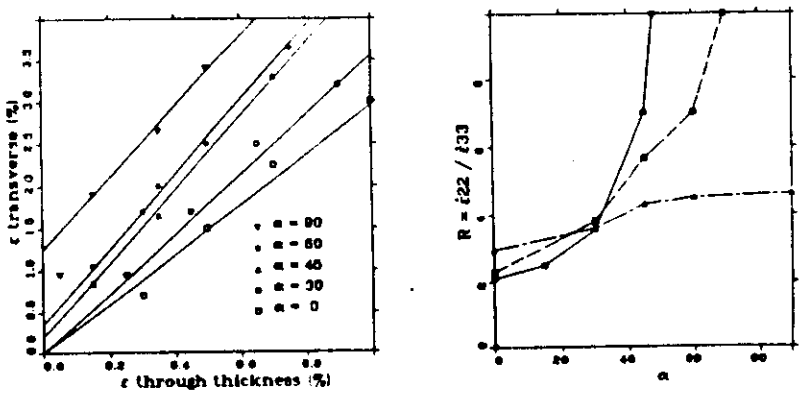


Figure 3: Transverse plastic component plotted versus through thickness component for different values of α.

Figure 4: Lankford coefficient as a function of the angle α: (- - -) experimental initial trend, (-.-.-) experimental stable values, ( _____ ) predicted values.

It is interesting to observe that the experimental values of R also show a singular behavior at low strains (see Fig.3) for α larger than 60°. Nevertheless this tendency seems to be rapidly overcame during the deformation and finite positive values of R are measured. As for the mechanisms responsible for this behavior, the evidence provided by texture and electron microscopy observations suggests that even at small strains a non negligible reorientation and important changes in the microstructure take place. After 7% deformation in the TD a tensile specimen shows a reorientation of the basal poles of 10° towards the ND and formation of cell walls of prism dislocations (9,10). As a consequence, not only the size but also the shape of the yield locus will evolve with deformation. Actually, if a reorientation of 10° is assumed to be present in all the tests, the PCYS calculated using this texture is in striking agreement with the experimental values as can be judged from Fig.2d .

## Conclusions

Self consistent calculations provide a reasonable prediction of the PCYS of rolled Zrly-4 with most of the deformation being accomodated by prismatic slip. Nevertheless, the Lankford coefficient seems to be more sensitive to details of the calculation. The fact that both self consistent and Taylor schemes fail to reproduce the observed behavior indicates that significant mechanisms may not be accounted for in the modelization. Among the possible candidates are: the evolution of texture and microstructure and elasto-plastic effects which for this material extend up to strains of 2% (7), indicating that elastic accomodation may be significant in that range.

Another important conclusion is that because of the rapid texture and hardenning evolution observed, the plastic characterization of rolled Zrly-4 provided by these tests may hold only in a small strain range. As a consequence, this information may not suffice to predict the formability performance of the material.

## Acknowledgments

This work was partially supported by the Proyecto Multinacional de Investigacion y Desarrollo en Materiales (OEA-CNEA) and the Franco-Argentinian Scientific Cooperation. One of us (C.T.) wish to acknowledge the hospitality of the Center for Materials Science, Los Alamos National Laboratory, where part of the work was developed.

## References

(1) C.Tome and U.F.Kocks, Acta Metall., 33 (1985) 603.

(2) N.Mingolo, A.Pochettino and C.Tome, (Presented at the 1er Simposio Franco-Argentino, Ciencia de Materiales, Mar del Plata, Argentina, 1986), 63.

(3) G.R.Canova, U.F.Kocks, C.Tome and J.J.Jonas, J.Mech. Phys. Solids, 33 (1985) 371.

(4) A.Molinari, G.R.Canova and S.Ahzi, Acta Metall., in press.

(5) S.Ahzi, A.Molinari and G.R.Canova, this conference.

(6) E.Tenckhoff, Met. Trans., 9A (1978) 1401.

(7) S.R.MacEwen, N.Christodoulou, C.Tome, J.Jackman, T.M.Holden, J.Faber Jr and R.L.Hitterman, this conference.

(8) C.Tome, S.Ahzi and G.R.Canova, this conference.

(9) P.Vedoya, A.Pochettino and R.Penelle, Textures and Microstructures, in press.

(10) A. Pochettino, P.Vedoya and R.Penelle, Constitutive Relations and their Physical Basis, (S.I.Andersen et al eds., RISO Nat. Lab., 1987), 485.

*Acta metall.* Vol. 37, No. 3, pp. 979–989, 1989
Printed in Great Britain

0001-6160/89 $3.00 + 0.00
Pergamon Press plc

# RESIDUAL STRESSES IN ANNEALED ZIRCALOY

**S. R. MacEWEN, C. TOME† and J. FABER Jr‡**
Advanced Materials Research Branch, Chalk River Nuclear Laboratories, Chalk River, Ontario, Canada K0J 1J0

(*Received* 7 *March* 1988)

**Abstract**—Neutron diffraction has been used to measure the lattice constants of single crystal and rod-textured polycrystalline Zircaloy-2 in the temperature range 300–900 K. While the single crystal remains strain-free during heating or cooling, large residual grain-interaction strains occur in the polycrystalline sample as the result of compatibility being maintained among grains with anisotropic thermal expansion coefficients. These residual thermal strains have been determined as a function of temperature from the difference between the single and polycrystal lattice constants. Analysis of the data has been done using a polycrystalline deformation model, QUEST, which accounts for anisotropic elasticity, plasticity and thermal expansion, and for the crystallographic texture of the sample. It is found that slow cooling from 900 K introduces residual stresses of the order of 100 MPa in the polycrystalline sample. The calculations demonstrate that these residual stresses can explain not only the difference in the proportional limits in tension and compression (strength differential) but also differences in the initial work hardening behaviour when Zircaloy-2 is deformed in tension or compression.

**Résumé**—La diffraction des neutrons a été utilisée, entre 300 et 900 K, pour mesurer les constantes réticulaires du Zircaloy-2 à l'état monocristallin et à l'état polycristallin avec une texture de barreaux. Alors que le monocristal ne subit pas de déformation en cours de chauffage ou de refroidissement, de grandes déformations résiduelles provenant de l'interaction des grains apparaissent dans le polycristal par suite du maintien de la compatibilité entre des grains dont les coefficients de dilatation thermique sont anisotropes. Ces déformations thermiques résiduelles ont été déterminées en fonction de la température, à partir de la différence entre les constantes réticulaires du mono- et du polycristal. Les résultats ont été analysés à l'aide d'un modèle de déformation d'un polycristal, QUEST, qui tient compte de l'élasticité anisotrope, de la plasticité et de la dilatation thermique, ainsi que de la texture cristallographique de l'échantillon. Un refroidissement lent à partir de 900 K introduit des contraintes résiduelles d'environ 100 MPa dans l'échantillon polycristallin. Les calculs montrent que ces contraintes résiduelles peuvent expliquer non seulement la différence entre les limites de proportionnalité en traction et en compression (différentiel de résistance mécanique), mais encore des différences d'écrouissage initial selon que le Zircaloy-2 est déformé en traction ou en compression.

**Zusammenfassung**—Die Gitterkonstanten von Ein-und Polykristallen (mit Stabtextur) der Legierung Zirkaloy-2 wurde im Temperaturbereich zwischen 300 und 900 K mittels Neutronenbeugung gemessen. Während der Einkristall beim Aufheizen und Abkühlen spannungsfrei bleibt, treten im Polykristall zwischen den Körnern wegen deren anisotropen thermischen Ausdehnungskoeffizienten und aus Kompatibilitätsgründen große Restspannungen auf. Diese thermischen Restspannungen wurden aus den Unterschieden zwischen Einkristall- und Polzkristallkonstanten in Abhängigkeit von der Temperatur ermittelt. Die Daten wurden mit einem Modell der Verformung von Polykristallen, QUEST, ausgewertet. Dieses Modell berücksichtigt anisotrope Elastizität, Plastzität, thermische Ausdehnung und kristallografische Textur der Probe. Es ergibt sich, daß langsames Abkühlen von 900 K Restspannungen in der Größenordnung von 100 MPa in den Polykristall einführt. Die Berechnungen zeigen, daß diese Restpannungen nicht nur den Unterschied in der Proportionalitätsgrenze im Zug und Druck, sondern auch Unterschiede in der Anfangsverfestigung bei Verformung in Zug oder im Druck der Zirkaloy-2-Legierung erklären können.

## 1. INTRODUCTION

In alloys with anisotropic thermal properties, thermal expansion or contraction will depend on crystallographic direction and, in general, elastic strains must be present to maintain compatibility between adjacent grains. As a consequence, treatments such as annealing, which supposedly remove residual stresses, will instead give rise to a state of internal stress in each grain. In 1968, Piercy [1] made the first attempt to calculate the residual thermal stresses that would result from heating or cooling Zr. His calculation was based on knowing the difference between the average thermal expansion coefficients of the polycrystalline sample and the individual coefficients for a single grain. Piercy's result was that for one degree of cooling, the basal planes would be left 0.21 MPa in tension, while the prism planes would be under a compressive stress of 0.15 MPa. While the role played by residual macro-stresses in the per-

†Instituto de Fisica Rosario, UNR, Av. Pellegrini 250, 2000 Rosario, Argentina.
‡Materials Science Division, Argonne National Laboratory, Argonne, IL 60439, U.S.A.



-7-

formance of engineering materials is well recognized, it is only recently that the influence of residual grain–interaction stresses on the behaviour of zirconium and titanium alloys has been appreciated. Recent calculations [2, 3] suggest that residual grain–interaction stresses produced by thermo-mechanical treatment are responsible for transients observed [4] in the irradiation growth behaviour of zirconium alloy pressure tubes.

This work will present direct measurements of residual thermal strains in Zircaloy-2, and will compare the results with an analysis based on the elastic, plastic and thermal properties of Zr alloy crystals. The basis of the experiment is to use neutron diffraction to measure the lattice parameters of a single crystal and a polycrystalline sample of Zircaloy-2 as a function of temperature. Any difference is a direct measure of the elastic strain required to maintain compatibility among the grains of the polycrystalline bar. Also, it will be shown that the yield stress differential between tension and compression along the axis of Zircaloy bar can be explained entirely when thermal stresses are taken into account.

## 2. EXPERIMENTAL

Many attempts were made to grow single crystals of Zircaloy using the standard, electron-beam, floating zone technique that had proved successful for growing crystals of Zr. All proved futile, with the result of the zone pass being a rod with large grains. The crystal used for the diffraction experiments grew by chance to a size approximately 4 × 5 × 4 mm. This grain was cut from the rod, chemically polished, and X-rayed in rotation steps of about 20° to ensure that it was indeed a single crystal.

The polycrystalline sample was cut from swaged rod and annealed 4 h at 925 K to produce equiaxed grains with an average diameter of 20 $\mu$m. Figure 1(a) shows the basal, (0002), pole figure obtained by neutron diffraction. The texture is almost perfectly axisymmetric, with the majority of grains having their $\langle c \rangle$ direction normal to the axis of the rod. The $(11\bar{2}0)$ pole figure shown in Fig. 1(b) indicates a very strong preference for these prism poles to align with the axis of the rod.

The neutron diffraction experiments were done using the time-of-flight General Purpose Powder Diffractometer at the Intense Pulsed Neutron Source

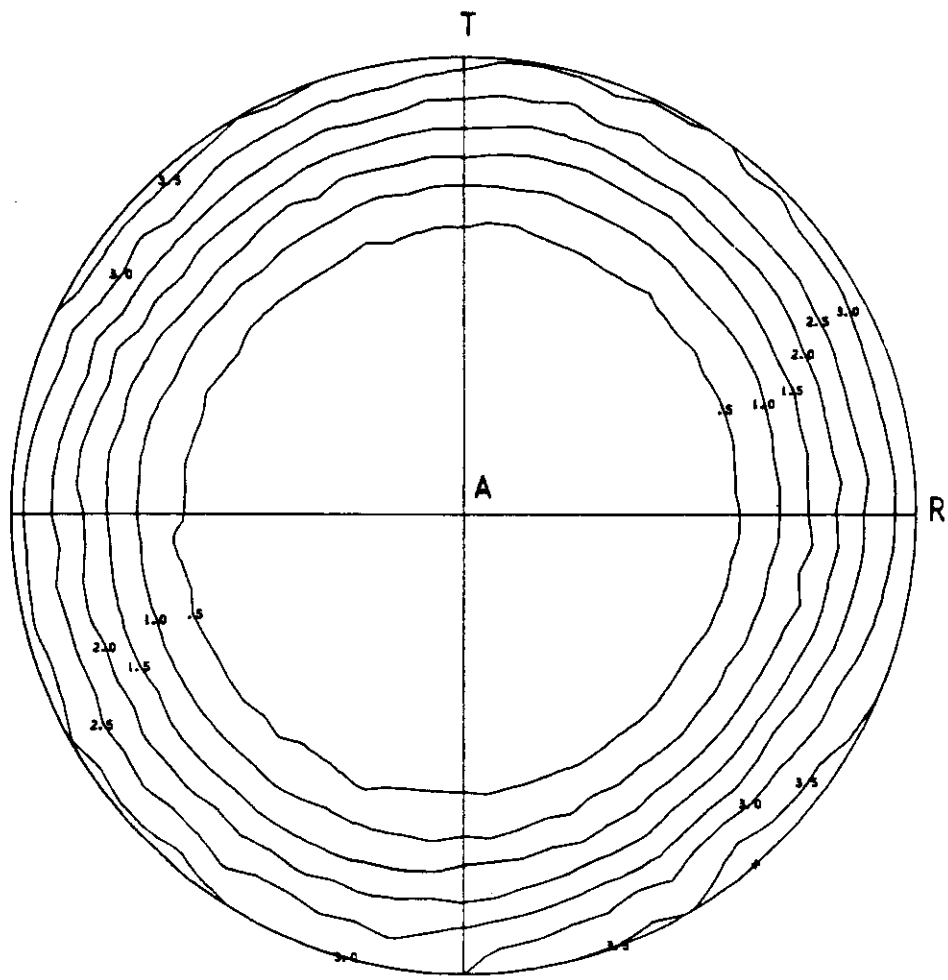


Fig. 1(a) *Caption on facing page*

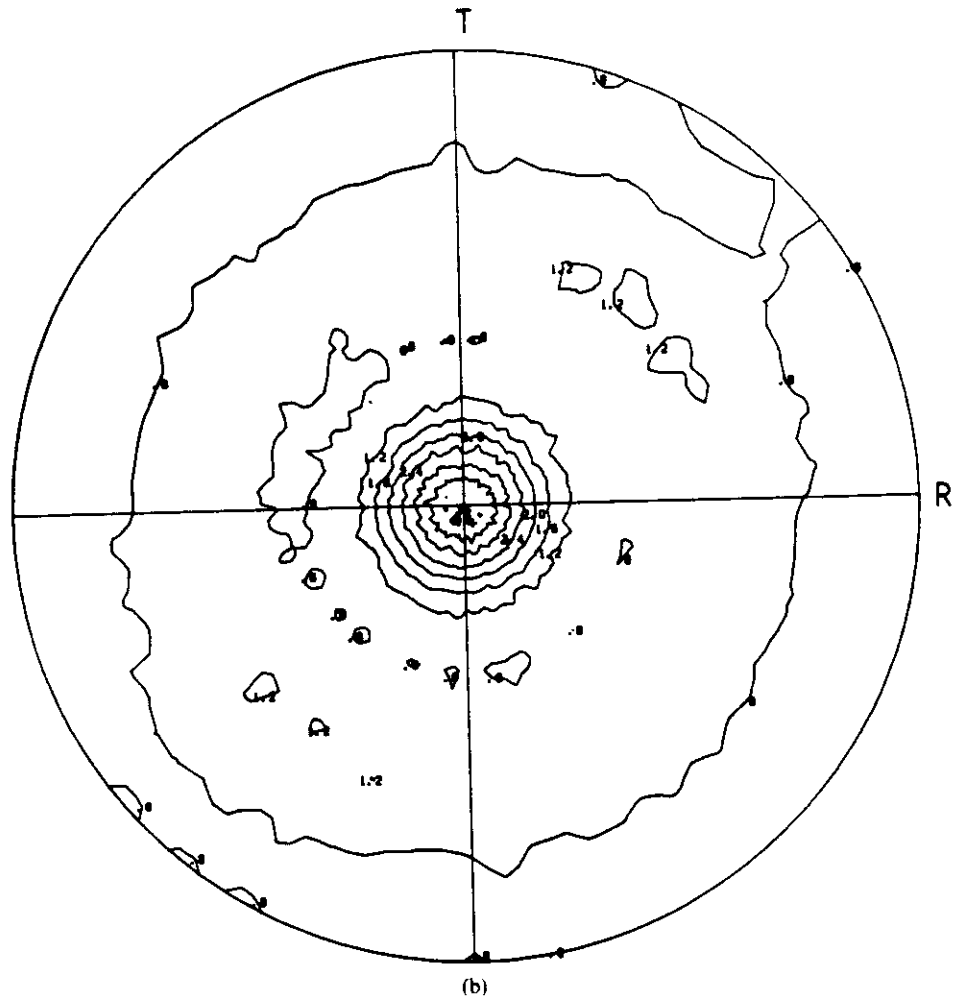


(b)

Fig. 1. Basal (0002) and prism ($11\bar{2}0$) pole figures for rod-textured Zircaloy-2: (a) (0002) (b) ($11\bar{2}0$). The axial direction of the rod is at the center of the pole figure.

(IPNS) at the Argonne National Laboratory in Chicago [5]. A small, Ta-wound furnace with slits to allow for the incident and $\pm 90^{\circ}$ diffracted beams was located at the centre of the diffractometer. The sample was suspended on a thin-walled alumina tube in the centre of the furnace. Temperature was monitored and controlled by two thermocouples in contact with the top and bottom of the polycrystalline rod, or with the vanadium post on which the single crystal was mounted.

The single crystal was oriented in the beam so that the (0002) and higher order basal reflections went to the $+90^{\circ}$ bank of detectors, and the ($10\bar{1}0$) and higher order prism reflections to the $-90^{\circ}$ bank. The rod sample was positioned vertically in the diffractometer, thus only those grains having their diffracting plane normals within $\pm 3.5^{\circ}$ of the horizontal scattering plane would contribute to the diffraction pattern. The test procedure for each sample was as follows. The sample was heated to 900 K, allowed to equilibrate and a time-of-flight diffraction pattern was obtained. The sample was then cooled approximately 50 K and the equilibration and data collection steps were repeated. The sequence of cooling 50 K, equilibration, and data collection was repeated every 50 K from 900 to 300 K. The cooling step took about 20 min at high temperatures, and as long as 2 h at low temperature; data acquisition required approximately 4 h in order to obtain sufficient counts in the weak ($10\bar{1}0$) peak.

## 3. RESULTS

The basal and prism plane $d$-spacings are shown as a function of temperature in Fig. 2. It was found that the single crystal data were best described by a linear relationship, while a second order fit was marginally better for the polycrystalline data. The polycrystalline (0002) $d$-spacing is greater than that for the single crystal, indicating that cooling produces residual tension normal to the basal planes. The opposite is found for the prism planes: the larger $d$-spacing in the single crystal indicates residual compression normal to the prism planes in the polycrystal. The peak position (as defined by the mean of the function fitted to the experimental data) is determined by the aver-

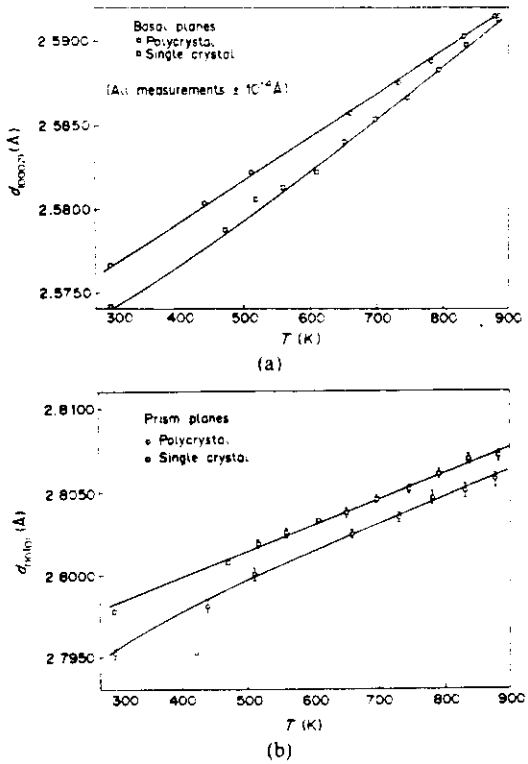


Fig. 2. Single crystal and polycrystal plane spacing of Zircaloy-2 as a function of the temperature: (a) (0002) planes; (b) $(10\bar{1}0)$ planes.

age of the $d$-spacings in the subset of grains oriented suitably for diffraction. A variation of (0002) $d$-spacing with rotation about the $\langle c \rangle$ pole is not expected to be significant, due to the basal-plane symmetry of the h.c.p. lattice. In general, however, the $(hikl)$ spacing is expected to depend on the orientation of the $\langle c \rangle$ pole with respect to the axis of the rod. Thus the mean position of the $(10\bar{1}0)$ peak is defined by the texture-weighted average of the $(10\bar{1}0)$ $d$-spacings of the diffracting grains.

Figure 3 plots the residual strains $\epsilon_{0002}$ and $\epsilon_{(10\bar{1}0)}$, given by

$$\epsilon^{\text{pol}}_{(hikl)} = \frac{d^{\text{pol}}_{(hikl)} - d^{\text{sc}}_{(hikl)}}{d^{\text{sc}}_{(hikl)}}.$$

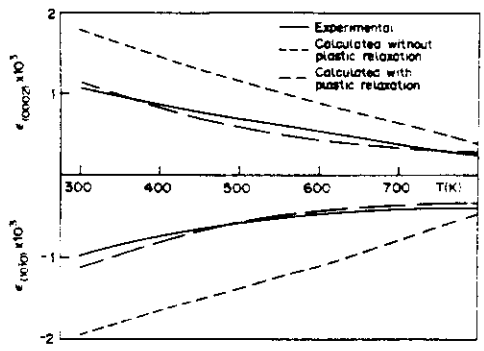


Fig. 3. Measured and calculated residual thermal strains as a function of the temperature.

Curvature is clearly evident, with the rate of increase of the residual strains increasing with decreasing temperature. Cooling from 900 K is seen to produce residual strains of the order of $10^{-3}$ at room temperature, with the basal planes in tension and the prism planes in compression.

## 4. ANALYSIS

When a polycrystalline metal is subjected to surface tractions or a change in temperature, the constituent grains undergo a change in shape and, because of the constraints imposed by the neighbouring grains and the requirement of compatibility, develop a state of internal stress. The grain interactions are complicated and in modelling the polycrystalline deformation a number of restrictive assumptions have to be made. In particular, the Taylor assumption and the concept of the "single crystal yield surface" are the cornerstones of the analysis employed in this paper and are described in detail elsewhere [6].

The polycrystalline sample is modeled as a discrete collection of grains. Each grain is defined by a set of Euler angles $(\Phi, \Theta, \omega)$ describing the orientation of the crystal axes with respect to the sample axes (see Fig. 4) and a weight $w(\Phi, \Theta, \omega)$ which represents the volume fraction of material so oriented. A thermomechanical test is simulated by means of successive strain and/or temperature increments imposed upon the grains. The Taylor assumption requires that the *total strain increment* has to be the same for every grain and equal to the strain increment of the sample. This hypothesis automatically ensures compatibility and represents an upper limit for the real stress–strain

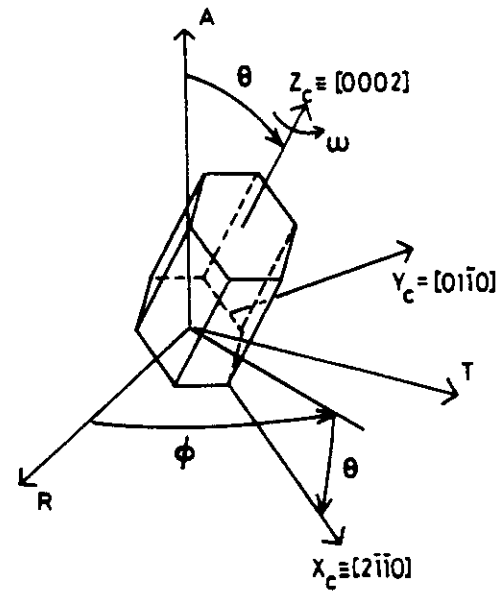


Fig. 4. Euler angles convention used in this work to describe the orientation of the crystal axes with respect to the sample axes. The arrows give the direction of rotation; the origin is defined when the two coordinate systems are coincident.

behaviour of the polycrystal [7]. The elastic, plastic and thermal contributions are allowed to differ from grain to grain, depending on the orientation, such that

$$\Delta\epsilon_{ij}^{T} = \Delta\epsilon_{ij}^{el} + \Delta\epsilon_{ij}^{pl} + \Delta\epsilon_{ij}^{th} \quad (1)$$

The stress in the grain is linearly related to the elastic strain tensor through Hooke's law

$$\sigma_{ij} = C_{ijkl}\epsilon_{kl}^{el}. \quad (2)$$

The thermal strain increment is proportional to the temperature increment $\Delta T$

$$\Delta\epsilon_{ij}^{th} = \alpha_{ij}\Delta T \quad (3)$$

where $\alpha$ is the tensor of thermal expansion coefficients. The stress is kept within the bounds of the single crystal yield surface defined by the yield condition (Schmid law)

$$\sigma_{ij}b_i^{(s)}n_j^{(s)} = \tau^{(s)}. \quad (4)$$

Here $\tau^{(s)}$ is the critical resolved shear stress in the system (s), $n^{(s)}$ is the normal to the slip plane and $b^{(s)}$ is the slip direction. Whenever the condition (4) is fulfilled the system shears plastically by an amount $\Delta\gamma^{(s)}$ related to the plastic strain increment through

$$\Delta\epsilon_{ij}^{pl} = \tfrac{1}{2}[b_i^{(s)}n_j^{(s)} + b_j^{(s)}n_i^{(s)}]\Delta\gamma^{(s)}. \quad (5)$$

In a typical simulation of a thermomechanical test, strain is imposed incrementally to every grain, starting from a stress-free state. At the beginning of the sequence every grain accommodates the thermal or externally imposed strain elastically, so building up internal stresses. Eventually, the stress reaches the single crystal yield surface and plastic deformation is triggered in at least one slip system. As deformation proceeds the stress vector "slides" across the yield surface and other systems are activated until the stress reaches a five-fold corner (vertex) of the yield surface. Unless some form of work hardening is considered, the elasto–plastic transition comes to a halt in the grain and any further deformation will be accommodated fully plastically. Clearly, the extent of the elasto–plastic transition will differ from grain to grain depending on its orientation.

A computer code called QUEST has been developed to calculate the stress–strain history of each grain for a given thermomechanical test. The initial total strain increment tensor is estimated, based on the nature of the test, and the elastic, plastic and thermal components of strain and the stress tensor are calculated for each grain. The average stress components in the sample are then compared with the boundary conditions of the test. If equilibrium is not fulfilled, the form of the strain increment tensor is modified and the entire procedure is repeated. Because of the linearity of the equations involved (equations 1–5), if boundary conditions on $N$ stress components are specified, the correct strain increment can be interpolated after performing $(N + 1)$ iterations with "trial" strain increments.

Figure 5 summarizes the input and output from the code. There are five main areas of input, described as follows in connection with the specific calculation dealt with in this paper:

(1) *Elastic properties.* Here the required input is the fourth order tensor of stiffness coefficients $C_{ijkl}$ given as a function of the temperature. The values measured by Fischer and Renken [8] for zirconium single crystals are assumed to be valid for Zircaloy crystals and are used in this paper. The temperature dependence of each coefficient is represented by means of a cubic polynominal fitted to the experimental values in the range $300\ \text{K} < T < 900\ \text{K}$.

(2) *Thermal properties.* In this case, the second order tensor of single crystal thermal expansion coefficients is required. Because of the hexagonal symmetry, only two diagonal components are independent and the non-diagonal components are zero. The values used here are derived from the slope of the single crystal curves of Fig. 2. They are:

$$\alpha_{11} = \alpha_{22} = 5.7 \times 10^{-6}\ \text{K}^{-1}$$

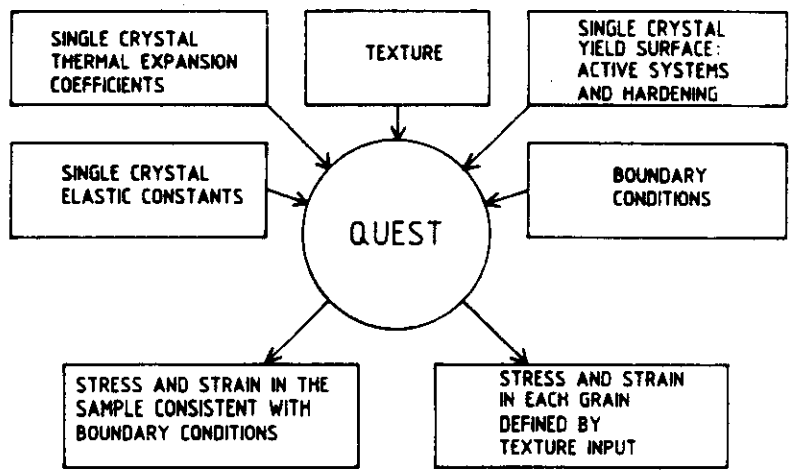


Fig. 5. Input and output information related to the computer code QUEST.

and

$$\alpha_{33} = 11.4 \times 10^{-6}\,\mathrm{K}^{-1}.$$

(3) *Texture*. Here one must define the number of grain orientations that, together with the corresponding weights, is sufficient to model the actual texture and the response of the polycrystal. As will be demonstrated in what follows, the cylindrical symmetry of the rod texture shown in Fig. 1 greatly reduces the number of grains necessary to represent the sample.

According to our convention (Fig. 4) the orientation of the basal poles with respect to the sample axes are described by the Euler angles $\Phi$ and $\Theta$, while the orientation of the prism planes is described by the angle $\omega$. The distribution of prism poles is such that in about two thirds of the grains the $\langle 10\bar{1}0\rangle$ axis is perpendicular to the axis of the rod, and in the remaining one third the $\langle 11\bar{2}0\rangle$ is normal to the rod axis. Since the elastic, plastic and thermal properties are essentially isotropic in the basal plane, it will be assumed that for a given orientation of the $\langle c\rangle$ axis, only grains with the "$\langle 10\bar{1}0\rangle$" orientation ($\omega = 0^\circ$) are present in the polycrystal. This assumption reduces by a factor of two the number of grains needed to model the texture and means that $\Phi$ and $\Theta$ suffice to describe the thermomechanical response of the grain. The average stress in the sample will be given by

$$\langle \sigma_{ij}\rangle^{SA} = \frac{1}{\Phi_0}\int_{\Phi=0}^{2\pi} \times \int_{\Theta=0}^{\pi/2} \sigma_{ij}^{SA}(\Phi,\Theta) I(\Phi,\Theta)\sin\Theta\, d\Theta\, d\Phi \quad (6)$$

where $\sigma_{ij}^{SA}(\Phi,\Theta)$ is the stress (expressed in sample axes) in the grains having the $c$-axis in the direction defined by $\Phi$ and $\Theta$; $I(\Phi,\Theta)$ is the intensity of basal poles, as measured by diffraction in that direction and $\Phi_0$ is a normalization constant defined as

$$\Phi_0 = \int_{\Phi=0}^{2\pi}\int_{\Theta=0}^{\pi/2} I(\Phi,\Theta)\sin\Theta\, d\Theta\, d\Phi. \quad (7)$$

The cylindrical symmetry of both *the texture and the testing constraints* ensures that: (i) the intensity of basal poles will be independent of $\Phi$, such that $I = I(\Theta)$ and (ii) the stress state will be identical (when referred to crystal axes) in all the grains that belong to a fiber at constant $\Theta$. When expressed in sample coordinates these stress states will differ in a rotation $\Phi$ around the sample axis. As a consequence, the contribution of a fiber to the average stress can be expressed in terms of the stress state in a single grain in the fiber (say $\sigma^{SA}_{\Phi=0,\Theta}$). The integration over $\Phi$ in equation (6) can be carried out explicitly for each stress component and as a result

$$\langle \sigma_{11}\rangle^{SA} = \langle \sigma_{22}\rangle^{SA} = \frac{2\pi}{\Phi_0}\int_{\Theta=0}^{\pi/2} \times \frac{\sigma_{11}^{SA}(\Theta)+\sigma_{22}^{SA}(\Theta)}{2} I(\Theta)\sin\Theta\, d\Theta$$

$$\langle \sigma_{33}\rangle^{SA} = \frac{2\pi}{\Phi_0}\int_{\Theta=0}^{\pi/2} \sigma_{33}^{SA}(\Theta) I(\Theta)\sin\Theta\, d\Theta$$

$$\langle \sigma_{12}\rangle^{SA} = \langle \sigma_{13}\rangle^{SA} = \langle \sigma_{23}\rangle^{SA} = 0. \quad (8)$$

When the continuum distribution of orientations is replaced by a discrete distribution defined by $\Theta_n$ and $\Delta\Theta_n$, the integrals adopt the form of a summation

$$\langle \sigma_{11}\rangle^{SA} = \langle \sigma_{22}\rangle^{SA} = \sum_{n=1}^{N} \frac{\sigma_{11}^{SA}(\Theta_n)+\sigma_{22}^{SA}(\Theta_n)}{2} W_n$$

$$\langle \sigma_{33}\rangle^{SA} = \sum_{n=1}^{N} \sigma_{33}^{SA}(\Theta_n) W_n \quad (9)$$

where

$$W_n = \frac{I(\Theta_n)\sin\Theta_n \Delta\Theta_n}{\sum_n I(\Theta_n)\sin\Theta_n\Delta\Theta_n} \quad (10)$$

represents the relative weight (volume fraction) of the grains in the $\Theta_n$ fiber. Observe that the cylindrical symmetry has reduced the number of orientations necessary to represent the sample to only those characterized by different values of $\Theta$. In this work five orientations are considered, all with $\Phi = 0^\circ$ and the $\langle 10\bar{1}0\rangle$ poles perpendicular to the rod axis ($\omega = 0^\circ$). The basal poles $\langle 0002\rangle$ are arranged as a "fan" at angles $\Theta_n = 50^\circ, 60^\circ, 70^\circ, 80^\circ$ and $90^\circ$. The weight assigned to each orientation is calculated using equation (10) with the intensities from the pole figure depicted in Fig. 1(a). The texture data are summarized in Table 1. Comparison with the measurements of prism plane spacing obtained by neutron diffraction has to be done with the weighted average of the strain component $\epsilon_{22}$ in each of the five grains using the normalized intensity, $I(\Theta)\Delta\Theta$, and not the volume fraction $[W(\Theta)]$ as the weighing factor.

(4) *Plasticity*. A complete characterization of the single crystal yield surface and its dependence on workhardening is required. Here one has to identify the potentially active systems and how their critical resolved shear stresses depend on temperature and on accumulated strain. For the analysis to follow the yield surface is defined by the six $\{10\bar{1}0\}\langle 1\bar{2}10\rangle$ prism slip systems and the 25 $\{10\bar{1}1\}\langle 11\bar{2}3\rangle$ pyramidal slip systems. There is no experimental evidence of twinning being significantly active during the process that we want to describe and for this reason deformation by twinning is excluded from the analysis.

Table 1. Orientations, basal pole intensities and corresponding fibre volume fractions used in this work to represent the rod texture as depicted in Fig. 1

| $n$ | $\Phi_n$ | $\Theta_n$ | $\omega_n$ | $I(\Theta_n)$ | $W(\Theta_n)$ |
|---|---|---|---|---|---|
| 1 | 0 | 50 | 0 | 0.1 | 0.016 |
| 2 | 0 | 60 | 0 | 0.3 | 0.054 |
| 3 | 0 | 70 | 0 | 0.9 | 0.174 |
| 4 | 0 | 80 | 0 | 2.1 | 0.425 |
| 5 | 0 | 90 | 0 | 3.2 | 0.330 |

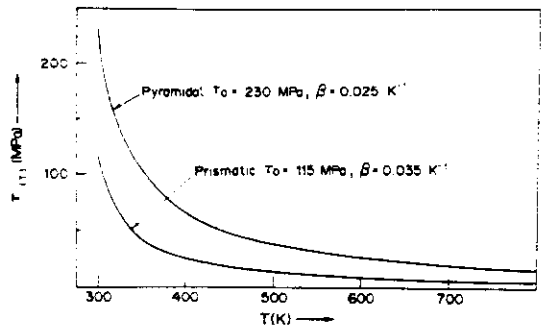


Fig. 6. Temperature dependence of the prism and pyramidal critical resolved sheer stresses assumed for the analysis.

Ideally one would like to have independent measurements of the prism and pyramidal critical stresses for single crystals of Zircaloy as a function of temperature. Since no such data exist, it is assumed that the temperature dependence of the critical shear stresses can be described by an empirical equation of the form

$$\tau_{(T)} = \frac{\tau_0}{1 + \beta(T - T_0)} \tag{11}$$

where the critical stress at room temperature, $\tau_0$, and the temperature sensitivity $\beta$ are adjustable parameters. Equation (11) is meant to provide a simple phenomenological description of the inverse dependence of CRSS on temperature such as observed by Akhtar [9] in zirconium. The critical resolved shear stresses used in the analysis are plotted in Fig. 6 and correspond to values of $\sigma_0^{PR} = 115$ MPa, $\sigma_0^{PY} = 230$ MPa, $\beta^{PR} = 0.035\,K^{-1}$ and $\beta^{PY} = 0.025\,K^{-1}$. These have been chosen so as to provide a reasonable fit to the measured residual thermal strains of Fig. 3 and to the flow stresses of the tensile stress–strain curve. At room temperature the critical resolved shear stress for pyramidal slip is twice that for prismatic slip.

Slip systems are assumed to harden linearly with the total accumulated shear according to a law

$$\Delta\tau^{(s)} = h^{(s)} \sum_s \Delta\gamma^{(s)}$$

Different hardening rates, $h^{(s)}$, are assumed for prismatic and for pyramidal systems, with numerical values obtained by comparison with the experimental workhardening rates from the tensile stress–strain curve.

(5) *Boundary conditions*. The boundary conditions imposed upon the average stress components given by equation (9) are characteristic of the type of test being simulated. During cooling the sample is left free to deform in any direction and as a consequence the strain increments have to be such that $\langle\sigma_{11}\rangle = \langle\sigma_{22}\rangle = \langle\sigma_{33}\rangle = 0$. During a tensile or compressive test along the axial direction of the rod, the component $\langle\sigma_{33}\rangle$ is a consequence of the imposed strain $\epsilon_{33}$, while $\epsilon_{11}$ and $\epsilon_{22}$ have to comply with $\langle\sigma_{11}\rangle = \langle\sigma_{22}\rangle = 0$ because the sample is not constrained laterally.

## 5. COMPARISON WITH EXPERIMENT

### 5.1. Thermal strains

The measured residual strains are compared with those calculated assuming no plastic relaxation in Fig. 3. For this calculation the critical resolved shear stresses were set to high values over the whole temperature interval in order to keep the stress state in all grains inside (an never touching) the yield surface. It is evident that when the grains are forced to accommodate the incompatibilities arising from differential thermal expansion elastically, the calculation significantly overpredicts the residual strains. At room temperature, values of $+1.78 \times 10^{-3}$ and $-1.93 \times 10^{-3}$ are predicted for the basal and prism plane strains respectively, while the experiment gives $1.04 \times 10^{-3}$ and $-0.97 \times 10^{-3}$, respectively. Figure 3 also shows the effect of allowing for plastic relaxation during the cooling process. If a dependence of the critical stress with temperature as depicted in Fig. 6 is assumed, then the yield surface expands as the temperature decreases (the distance of the facets to the origin is proportional to the critical stress). In the interval going from 800 to 500 K the CRSS's are low and the elastic strains required for compatibility cannot build up very far before the stress reaches a facet of the yield surface and triggers plastic flow. Thus, the rate of increase of residual strains at high temperatures is low because it is subordinated to the rate of increase of the yield surface. For temperatures lower than 500 K the critical stresses increase faster than the build up of internal stress as temperature drops. The strain incompatibilities are now accommodated entirely elastically and as a consequence the internal stresses increase at a higher rate than when some plastic accommodation was occurring. That the process at low temperatures is controlled elastically can be inferred from Fig. 3 where the final slopes are the same for the strains calculated with and without plastic relaxation. Nevertheless, it is evident that only by including plastic relaxation is there reasonable agreement between theory and experiment over the whole temperature range, even if at room temperature the calculated residual strains exceed the experimental values by about 10%.

The diagonal components of the stress tensor in every grain are plotted in Fig. 7 as a function of the titling of the $c$-axis with respect to the rod axis. Data correspond to room temperature and are expressed in crystal axes. It can be seen that the basal planes are in tension ($\sigma_{33} > 0$) in all the grains, the prism planes are in compression ($\sigma_{22} < 0$) and the levels of the residual stress are high ($\sim 100$ MPa). As will be shown in what follows, the residual thermal stresses at room temperature play an important role in retarding or accelerating the onset of plasticity during mechanical testing.

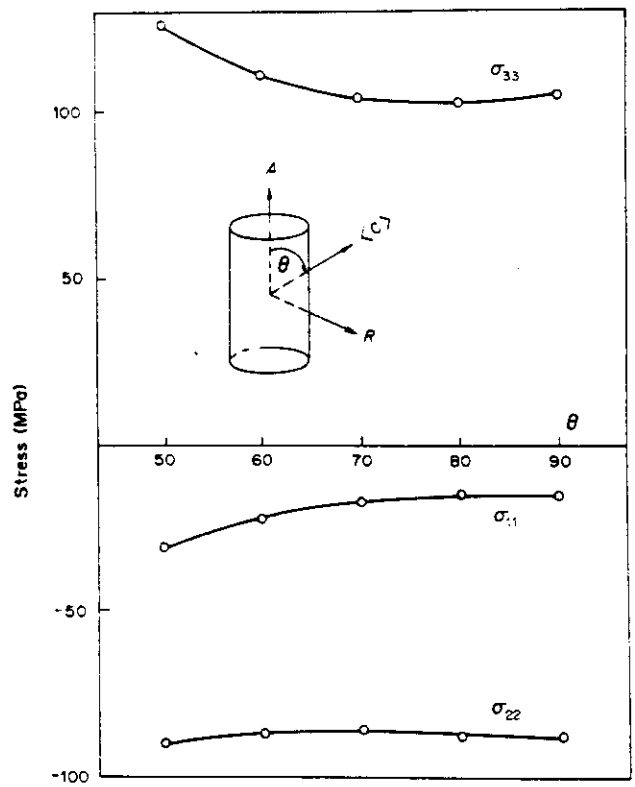


Fig. 7. Residual thermal stresses at room temperature as a function of the angle between the sample axis and the basal plane normal, $\langle c \rangle$.

*5.2. Mechanical behaviour*

The elasto–plastic response of the rod sample after cooling was analyzed theoretically and measured experimentally for axial tension and axial compression along the rod axis. The theoretical predictions are shown in Fig. 8, together with the curve that results when a strain free state at room temperature is assumed. In the latter case the curve is the same for tension and compression: the differences among the curves result entirely from the presence of the residual thermal strains. The experimental results are plotted in Fig. 9 and a number of interesting conclusions can be drawn from the comparison with the predicted stress–strain curves.

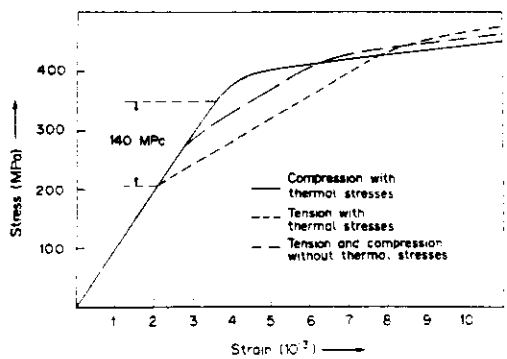


Fig. 8. Calculated stress–strain curves for tension and compression.

The elastic slope, which is the Young's modulus $E$ of the polycrystal, represents the weighted average of the elastic response of the constituent orientations. The fact that $E$ is correctly reproduced implies that the orientations and weights chosen for the analysis are a realistic representation of the rod texture. Even more important are the predictions of a strength differential of about 140 MPa between the proportional limits in tension and compression, and significant differences in the initial workhardening rates in tension and compression. Since the features of low yield stress and high initial hardening in tension, a high yield and low initial hardening in compression and a strength differential of 120 MPa are observed experimentally, it is reasonable to attribute their presence to the residual thermal stresses. Nevertheless, while the agreement in general features between theory and experiment is remarkable, the curves differ in the magnitude of the strength differential and the extent of the elasto–plastic interval. While the calculated elasto–plastic transition is over at about 1.0% strain, the measurements indicate that the material is not fully plastic until at least 2% strain. The reasons for these discrepancies are discussed in the following section.

The slope of the calculated stress–strain behaviour beyond the elasto–plastic transition results from assuming a hardening rate of $h^{PR} = 400$ MPa and $h^{PY} = 800$ MPa for prismatic and pyramidal systems

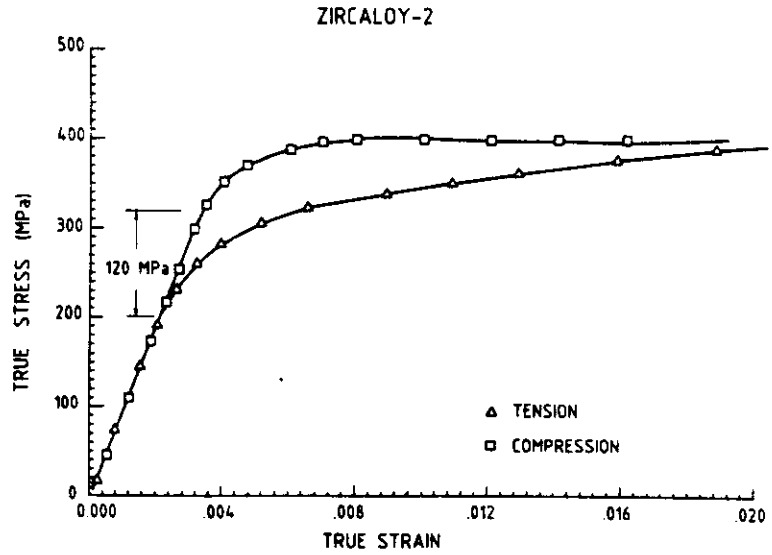


Fig. 9. Measured stress–strain curves for tension and compression along the rod axis.

respectively. If no hardening were considered all three curves would level (and stay) at the same value of flow stress once the material becomes fully plastic. As deformation proceeds, the thermal strains are gradually erased and replaced by a new state of internal strain which is characteristic of the mechanical test.

## 6. DISCUSSION

Two aspects of our results deserve further discussion: the mechanisms underlying the strength differential and the extent of the elasto–plastic range. According to our convention, the initiation of the elasto–plastic transition (and with it the yield stress) is defined by the first grain that starts deforming plastically and its termination corresponds to the situation where all the grains are fully plastic and no new slip systems will be activated thereafter. Neither extreme can be precisely identified in the experiment. From the calculations we are able to follow the evolution of stress and the order in which the slip systems are activated in each grain. When no residual thermal stresses are assumed, the calculation predicts (dashed curve in Fig. 8) that the elasto–plastic regime starts with the activation of prismatic slip in grains 3–5 within an interval of 0.1% deformation (see Table 2). It is not until the deformation reaches 0.6% that pyramidal slip is activated and at about 0.8% the polycrystal becomes fully plastic. The combination of plastic and elastic deformation explains why, before that point, the apparent hardening rate, $d\sigma/d\epsilon$, of the polycrystal is so high. The same behaviour is found during tension when residual strains are present (see Table 2), except that now yielding takes place at lower values of stress and the elasto–plastic transition for the polycrystal extends to about 1.0% deformation. When compression is simulated for a sample with thermal strains, the yield stress is higher and the onset of plasticity is characterized, within an interval of 0.1%, by the simultaneous activation of prism and pyramidal slip in grains 4 and 5 (see Table 2). After a total deformation of 0.5% grains 3 to 5 are fully plastic and the slope of the stress–strain curve is governed by the hardening of the deformation systems, without any further elastic contribution. It is worth pointing out here that the stress–strain behaviour of the polycrystal shown in Fig. 8 is mostly determined by the more heavily weighted grains, 4 and 5. The previous results admit a straightforward and clarifying explanation within the framework of the single crystal yield surface.

For the sake of argument, a sketchy deviatoric plane representation of the yield surface has been drawn in Fig. 10. The vertical facets correspond to prism slip and the inclined ones to pyramidal slip. Opposite facets represent slip in the same plane but in opposite directions (see for example Ref. [10]). The vector representing the total stress in each grain remains bounded by the yield surface. To start with, assume that the grain is initially free of residual stress. When the sample is loaded in tension the stress in the grain will evolve from the origin towards one of the

Table 2. Status of the grains that represent the sample at the onset of plasticity for different testing conditions. With and without refers to the inclusion or not of thermal strains respectively

| | Tension | | Compression | |
|---|---|---|---|---|
| Grain | With | Without | With | Without |
| 1 | Elastic | Elastic | Elastic | Elastic |
| 2 | Elastic | Elastic | Elastic | Elastic |
| 3 | 2 prism systems | 2 prism systems | 2 prism systems | 2 prism systems |
| 4 | 2 prism systems | 2 prism systems | 2 prism and 2 pyramidal systems | 2 prism systems |
| 5 | 2 prism systems | 2 prism systems | 2 prism and 4 pyramidal systems | 2 prism systems |

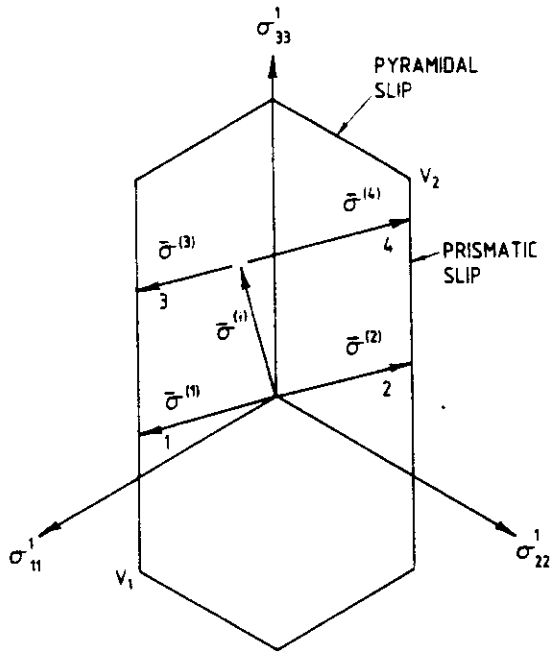


Fig. 10. Schematic representation of the evolution of the main stress components in grain No. 3 during tension and compression with and without thermal strains.

prismatic facets along path 1 in Fig. 10. Deformation will be entirely elastic until the stress vector achieves a value $\bar{\sigma}^{(1)}$ and prism slip is activated. It is not until the stress "slides" all the way down to the vertex $V_1$ (requiring a fairly large elastic contribution) that pyramidal systems will be activated. When the sample is loaded in compression the stress path in each grain is simply reversed (path 2), yield will take place in the opposite prism system for the same absolute value of stress and the grain will become fully plastic when the stress reached the vertex $V_2$. The effect of thermal strains is to create a state of internal stress $\bar{\sigma}^{(i)}$ which adds to the externally imposed stress to give the total stress in the grain. As a consequence, the symmetry under reversal of the imposed strain is now lost because of a shift in the apparent stress origin from the origin of the stress axes to a position defined by the vector $\bar{\sigma}^{(i)}$. For the particular case treated here a lower value of "external" stress $\bar{\sigma}^{(3)}$, [defined by the distance from $\bar{\sigma}^{(i)}$ to the prism facet along a path parallel to (1)], is required to achieve plastic flow in tension, while in compression the yield stress $\bar{\sigma}^{(4)}$, defined by the distance from $\bar{\sigma}^{(i)}$ to the first active facet along a path parallel to (2), increases. It is clear from this picture that the asymmetry introduced by the thermal stresses is responsible for the strength differential observed in the curves of Fig. 8. It is also clear that the extent of this differential is proportional to the magnitude of $\bar{\sigma}^{(i)}$ and its deviation with respect to the axis $\sigma_{33}$. The fact that our prediction exceeds the observed strength differential suggests that our predicted thermal stresses are not entirely correct. Another feature that can be easily explained using the simple picture of Fig. 10 is the different extent of the elasto–plastic transition in tension and compression. In the case of tension when thermal stresses are present the stress (and so the elastic strain) required to go from $\bar{\sigma}^{(3)}$ to the vertex $V_1$ is larger than to go from $\bar{\sigma}^{(1)}$, while for compression the distance from $\bar{\sigma}^{(4)}$ to $V_2$ is shorter than from $\bar{\sigma}^{(2)}$ and pyramidal slip is activated immediately after prismatic slip.

The difference between the predicted and measured strain of the elasto–plastic transition can be attributed to the use of the Taylor assumption. From a physical point of view, it is reasonable to assume that if a grain is "hard" in a given direction, the buildup of stress in that direction will trigger plastic flow in a "soft" neighbouring grain before reaching a facet of the yield surface in the "hard" grain. Macroscopic compatibility must still be satisfied, but now the total deformation will vary from grain to grain and the rate of build up of internal stress will be reduced. Calculations done by Hutchinson [7] using different polycrystalline models demonstrated that the elastic–plastic Taylor model, which essentially allows no relaxation, is an upper bound for the stress–strain curve of randomly oriented f.c.c. grains. In the other models the matrix is allowed to accommodate the difference between the plastic strain in the grain and the average plastic strain either elastically (Kroner [11] and Budianski and Wu [12] models) or elasto–plastically (Hill model [13]). The latter, characterized by a large degree of stress relaxation, would be expected to resemble more closely the real behaviour of the polycrystal, but its use is prohibitively complex. The comparison among the three models considered by Hutchinson shows that in order to achieve a given flow stress the KBW model requires about twice, and Hill's model about thrice the plastic strain predicted by Taylor's model. We expect that a similar conclusion will be valid for the case of textured h.c.p. polycrystals considered here. In such a case the present model will underestimate the plastic strain required for the elasto–plastic transition by at least a factor of two. Other features of the experimental curves of Fig. 10, such as the levelling of stress in compression is believed to be due to the early activation of twinning. This is the subject of work now in progress and will be addressed in a future paper, together with an analysis of the evolution of residual strains during plastic deformation.

## 7. CONCLUSIONS

Time of flight neutron diffraction has been used to determine the residual strains produced during cooling of rod-textured Zircaloy-2 and a code based on the Taylor assumption and the concepts of the single crystal yield surface has been developed for modeling the polycrystal behaviour. The comparison between predicted and measured results indicate that the residual stresses due to anisotropic thermal expansion become high enough to cause plastic flow during

cooling from 900 K to room temperature. It is shown that these residual stresses, which are of the order of 100 MPa, play a decisive role in determining the stress differential and the elasto–plastic transition in zirconium alloys. It is to be expected that they will also affect irradiation growth and the orientation of hydrides.

*Acknowledgements*—We would like to thank J. Watters and J. Mecke (Chalk River Nuclear Laboratories) and R. L. Hitterman (IPNS, Argonne National Laboratory) for their able technical assistance during the course of this work.

## REFERENCES

1. G. R. Piercy, *J. nucl. Mater.* **26**, 18 (1968).
2. R. A. Holt and A. R. Causey, *J. nucl. Mater.* **150**, 306 (1987).
3. A. R. Causey, R. A. Holt and C. H. Woo, *Proc. Int. Conf. Mech. Creep Growth*, Manitoba, Canada: 1987. *J Nucl. Mater.* To be published.
4. V. Fidleris, R. P. Tucker and R. B. Adamson, *ASTM STP 939*, 49 (1987).
5. A. W. Schulke and B. S. Brown, *IPNS User's Handbook* (1987).
6. S. R. MacEwen and C. Tome, *ASTM STP 939*, 631 (1987).
7. J. W. Hutchinson, *Proc. R. Soc.* **A319**, 247 (1970).
8. E. S. Fisher and C. J. Renken, *Phys. Rev.* **135**, A482–A494 (1964).
9. A. Akhtar, *J. nucl. Mater.* **47**, 19 (1973).
10. C. Tome and U. F. Kocks, *Acta metall.* **33**, 603 (1985).
11. E. Kroner, *Acta metall.* **9**, 155 (1961).
12. B. Budiansky and T. T. Wu, *Proc. 4th Congr. Appl. Mech.*, p. 1175 (1962).
13. R. Hill, *J. Mech. Phys. Solids* **13**, 89 (1965).

# THE EVOLUTION OF TEXTURE AND RESIDUAL STRESS IN ZIRCALOY-2

S.R. MacEwen, N. Christodoulou, C. Tome[1], J. Jackman[2], T.M. Holden*
Atomic Energy of Canada Limited
Chalk River Nuclear Laboratories
Advanced Materials Research Branch
*Neutron & Solid State Physics Branch
Chalk River, Ontario K0J 1J0 Canada

and

J. Faber Jr. and R.L. Hitterman
Materials Science & Technology
Argonne National Laboratory
9700 South Cass Avenue
ARGONNE, IL 60439 USA

## Abstract

The evolution of texture and residual grain-interaction strains during the compressive deformation of hcp Zircaloy-2 rod have been studied using neutron diffraction. The volume fraction of grains having their basal poles aligned with the rod axis increases continuously during deformation until, after 20% compression, the characteristic "rod-texture", with the basal poles normal to the axis, is replaced with a new texture having the basal poles aligned predominantly parallel to the axis of the rod. The residual strains initially evolve with the opposite sense to that observed previously for tensile deformation. However, after about 2% compression, evidence of a strong stress-relief mechanism is observed.

It will be demonstrated that all of the data can be explained by the effects of $(10\bar{1}2)\langle\bar{1}011\rangle$ deformation twinning. Calculations done using the code QUEST, which calculates polycrystal properties from single crystal parameters, show that the stress-relief produced by twinning is not consistent with the shear strain of the twins alone, suggesting that a relaxation strain, normal to the shear plane, is a significant feature of twinning in Zircaloy-2.

---

[1]Present address: Instituto de Fisica Rosario, UNR, Av. Pellegrini 250, 2000 Rosario, ARGENTINA.

[2]Present address: Physical Metallurgy Research Laboratories, CANMET, Energy, Mines & Resources, 568 Booth Street, OTTAWA, Ontario, K1A 0G1, Canada.

Eighth International Conference on
Textures of Materials (ICOTOM 8)
Edited by J.S. Kallend and G. Gottstein
The Metallurgical Society, 1988

## Introduction

The deformation of zirconium alloys is characterized by the evolution of residual grain-interaction stresses and the development of sharp crystallographic textures. Both are the consequence of the anisotropy of the single crystal yield surface, (SCYS). Zirconium alloys deform by slip on the six prism $(10\bar{1}0)\langle 11\bar{2}0\rangle$ systems and on the twenty-four pyramidal $(10\bar{1}1)\langle 11\bar{2}3\rangle$ systems. Akhtar [1] has shown that in crystal bar Zr, the critical resolved shear stress (CRSS) for pyramidal slip can be as much as 20 times that for prism slip; for Zircaloy-2, an alloy of Zr containing 1.5 wt% Sn and 1200 ppm oxygen in solid solution, the CRSS for pyramidal slip appears to be about twice that for prism slip. In either case, the SCYS is anisotropic, with the pyramidal facets further from the origin than the prism facets. Deformation twinning is produced readily in crystal bar Zr whenever the basal planes are in either tension or compression. Compression twins do not occur in Zircaloy-2, but twinning on the six $(10\bar{1}2)\langle\bar{1}011\rangle$ tensile systems occurs whenever the basal planes are deformed in tension [2,3]. According to the analysis to follow, it appears that the CRSS for twinning is slightly larger than that for pyramidal slip.

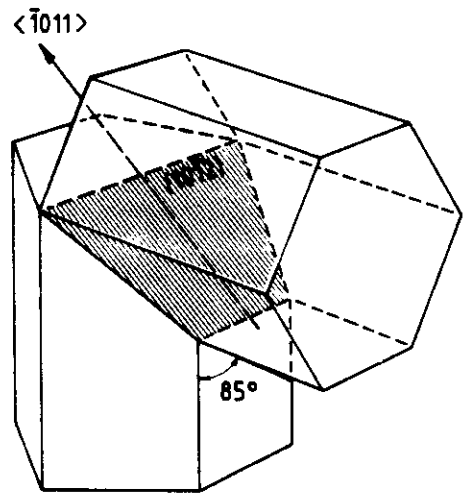


Figure 1 - Graphic representation of twinning in the $(10\bar{1}2)\langle\bar{1}011\rangle$ system occurring when the crystal is loaded in tension along the <c> direction.

Figure 1 illustrates the tensile twinning system which produces a rotation of the basal pole of ≈90° about a $\langle 11\bar{2}0\rangle$ direction. More precisely, the orientation of the twin with respect to that of the parent grain can be obtained by a rotation of $\pi$ about the $\langle\bar{1}011\rangle$ direction, giving the angle between the basal planes of the twin and parent grain as 85.2° [3].

The (0002), $(10\bar{1}0)$, and $(11\bar{2}0)$ pole figures of annealed Zircaloy-2 rod are shown in Figures 2a-2c. The axial direction of the rod is at the center of each pole figure. The texture is almost perfectly axisymmetric, with the basal poles lying predominantly in the RT plane (normal to the rod axis). Defining $\alpha$ as the angle between the axial direction of the rod and the direction of a basal pole, it is seen that most of the grains are oriented with $\alpha = 90° \pm 10°$; the basal pole intensity for $\alpha > 50°$ is negligible. Examination of the prism pole figures shows that about 2/3 of the grains have a $\langle 11\bar{2}0\rangle$ direction, and 1/3 a $\langle 10\bar{1}0\rangle$ direction, parallel to the rod axis.

Previous experiments [4,5] have shown that residual grain-interaction stresses are introduced into Zircaloy-2 rod by uniform slow cooling after annealing and by uniform uniaxial deformation. Within any fiber of the texture (defined by grains with a constant $\alpha$) the residual strain state, when expressed in <u>crystal coordinates</u> $\langle 2\bar{1}\bar{1}0\rangle$, $\langle 01\bar{1}0\rangle$, and $\langle 0001\rangle$, is identical for all grains as a result of the axisymmetry of the texture and the thermo-mechanical treatment. It is, therefore, most convenient to express residual grain-interaction strains or stresses in the <u>crystal coordinates</u> defined above. Similarly, texture can most easily be represented by plots of the texture coefficient, $T_c$, vs the polar angle $\alpha$.

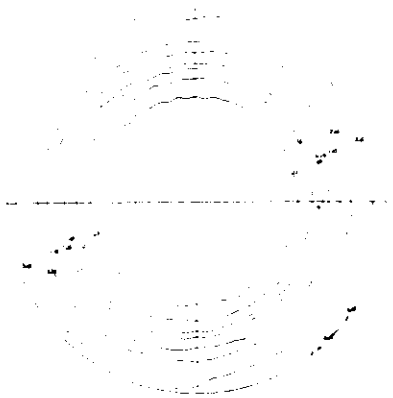

Figure 2(a)

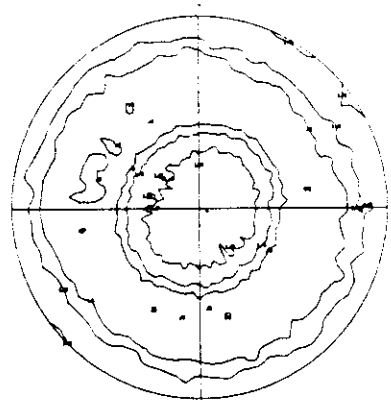

Figure 2(b)

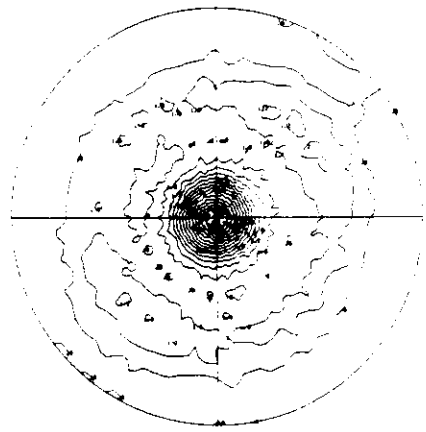

Figure 2(c)

Figure 2 - The (a) (0002), (b) $(10\bar{1}0)$ and (c) $(11\bar{2}0)$ pole figures of annealed Zircaloy-2 rod.

Cooling from an annealing temperature of 875 K produces residual strains of the order of $1 \times 10^{-3}$ (for the $\alpha = 90°$ fiber), with the basal planes in tension and the prism planes in compression [5,6]. These are the result of the anisotropy of the thermal expansion coefficients which are $5.7 \times 10^{-6}$ $K^{-1}$ for directions in the basal plane (isotropic) and $11.4 \times 10^{-6}$ $K^{-1}$ normal to the basal plane. The corresponding stresses are -95 MPa normal to the prism planes and +110 MPa normal to the basal planes. Residual stresses in the axial direction of the rod are negligible. These residual grain-interaction stresses are approximately 35% of the tensile yield and are responsible for the experimentally-observed strength differential [6].

The evolution of residual strains in bars, deformed initially in tension and consequently without deformation twinning occurring, has been determined previously [7] using neutron diffraction. Figure 3 plots the residual strains measured normal to the $(10\bar{1}0)$ $(11\bar{2}0)$, $(10\bar{1}2)$ and (0002) planes for grains in the $\alpha = 90°$ fiber. Points numbered 1 to 4 were obtained from samples deformed only in tension; points numbered 5 to 7 were determined from samples deformed 4% in tension and then various amounts, ranging from 1 to 3%, in compression. The strain axis of Figure 3 represents the net plastic strain in the sample. All diffraction measurements were made with the samples unloaded and values are given relative to an annealed (but not stress-free) reference sample. During

tensile deformation of the rod, the residual strains increase in tension normal to the prism planes and in compression normal to the basal planes. During reverse compressive flow, the residual strain state that evolved during tension is removed, and a new state, characteristic of compressive deformation is produced. The residual strains normal to the $(11\bar{2}0)$ planes are generally about 10% greater than those normal to $(10\bar{1}0)$, presumably as the result of a small plastic anisotropy in the basal plane.

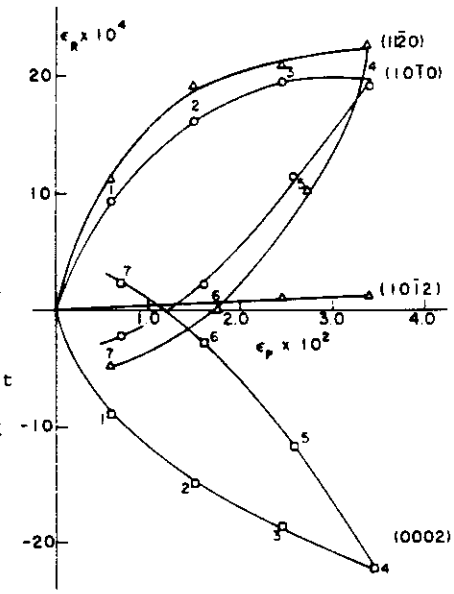


Figure 3 - Residual strains in tension measured to the $(11\bar{2}0)$, $(10\bar{1}0)$ and (0002) planes for grains with $\alpha = 90°$.

The objective of the work to be presented here is to evaluate the effect of deformation twinning, produced whenever rod samples are deformed initially in compression, on the evolution of texture and residual strain.

## Experimental

The material, as for previous experiments, was Zircaloy-2 rod, annealed for four hours at 925 K to give an equiaxed grain structure with average diameter of 20 $\mu$m. Test samples were either compression plugs 1.27 cm high with a 0.95 cm diameter, or tensile bars with a 1.9 cm gauge length and a 0.95 cm diameter. Compression tests up to 20% strain were performed on tensile bar samples using a MTS Alpha System. For higher compressive strains, the compression plugs were deformed between parallel platens, using teflon sheets for lubrication.

Texture measurements were made by neutron diffraction using the L3 triple-axis spectrometer at the NRU reactor at Chalk River. Since the measurement technique is completely non-destructive, a single compression plug sample was used to monitor texture evolution in compression. After a specified amount of deformation, the sample would be mounted on a Kappa goniometer and the intensity of the (hkil) diffraction peak would be measured in 5° increments over the complete hemisphere defined by the polar angle $\alpha$ and the azimuthal angle $\phi$. The background intensity was also measured over the complete hemisphere, allowing the raw data to be corrected for absorption and path-length effects before pole figures were calculated. The sample was positioned on the goniometer in precisely the same orientation, with a reference mark aligned with the incident beam, after each step of deformation. The statistics of the measurements were excellent, due to the large volume of the sample and thus the large number of grains contributing to diffraction; reproducibility of the texture coefficients was found to be $\pm 0.1$.

Residual grain-interaction strains were determined using time-of-flight neutron diffraction at the IPNS facility at the Argonne National Laboratory. Strains were calculated from the shifts in the positions of the diffraction peaks relative to those in the annealed reference sample. Details of the experimental procedure are given elsewhere [4]. The intensity of a given (hkil) peak, measured at a given (fixed-position) detector, originates from diffraction in a unique sub-set of grains which

have their diffracting plane normals in the scattering plane of the instrument and oriented to bisect the incident and diffracted neutron beams. The sample was positioned with the axial direction of the rod vertical in the diffractometer. Consequently, only those grains whose (hkil) plane normals were in the RT plane ($\alpha = 90°$) could have contributed to a diffraction pattern.

The twinned volume fraction in deformed samples was measured optically, using a quantitative IBAS-2 image analyzing system.

## Results

The stress-strain curves, shown in Figure 4, are significantly different in tension and compression. In tension, the proportional limit is lower and the initial workhardening rate is higher than in compression. After the initial transient, which lasts for about 3% in compression, the workhardening rate of the compression sample increases monotonically, while that of the tensile sample decreases with increasing flow stress.

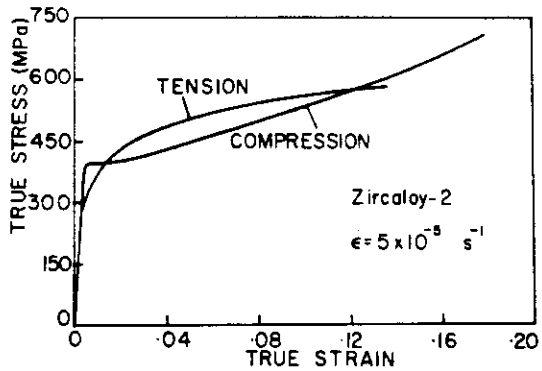


Figure 4 - Stress-strain curves of annealed Zircaloy-2 tested in tension and compression. Note the marked difference in the workhardening rate.

The twinned volume in the as-deformed samples increases linearly with increasing strain at a rate of about 2% per 1% strain, as shown in Figure 5. However, for strains less that about 2%, twins are rarely observed, even with transmission electron microscopy. Annealing the sample for four hours at 925 K decreases the twinned volume by about 50%, provided the strain is less that 10%. At higher strains the anneal causes recrystallization and a complete removal of the deformation twins.

Figure 6 shows the prism and basal pole figures after 20% compressive strain. Comparison with the as-annealed pole figures of Figure 2 reveals a remarkable rotation of the texture. The maximum basal pole intensity, which was initially normal to the axis of the rod, is now axial and the maximum prism pole intensities which were axial have rotated to lie in the RT plane. The axisymmetry of the pole figures has been maintained, consequently a plot of the texture coefficient vs $\alpha$ is a convenient way to illustrate the evolution of texture with plastic strain. Figures 7a-7c summarize the results for the (0002), ($10\bar{1}0$) and ($11\bar{2}0$) reflections, respectively. The maximum in basal pole intensity is approximately $T_c = 4$ after ~20% deformation. A recrystallization anneal increases this to $T_c = 16$, as shown in Figure 8. For comparison with the evolution of texture during compressive deformation, Figures 9a-9c show texture rotation after 15% tensile strain. The ($10\bar{1}0$) prism pole texture coefficient in the axial direction increases by a small amount, 0.7, while that of the ($11\bar{2}0$) poles decreases by the same amount; the basal pole intensities are essentially unchanged.

Figure 10 shows the evolution of residual grain-interaction strains during compression deformation of the rod. Comparison with Figure 3 reveals several features that differ from the evolution during tensile

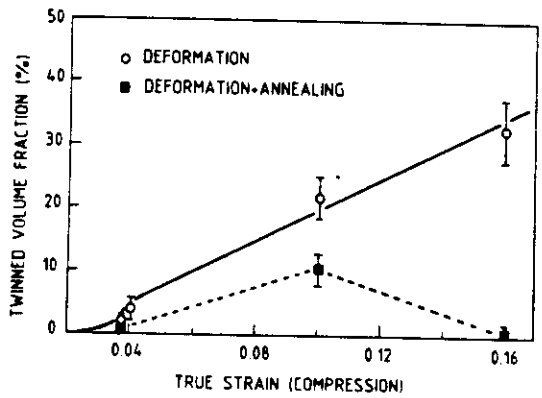


Figure 5 - Evolution of the twinning volume fraction as a function of compressive strain.

deformation. Overall, the residual strains are much lower. Initially, for the first 2% in compression, the evolution is more or less the opposite of that observed in tension; the strains normal to the (0002) planes increase in tension, while those normal to the prism planes, in the $\langle 10\bar{1}0\rangle$ and $\langle 11\bar{2}0\rangle$ directions, increase together in compression. Thereafter, the (0002) strains decrease while the prism strains increase. Most significant is the observation that the $(11\bar{2}0)$ behaviour no longer parallels that of the $(10\bar{1}0)$ planes. To the contrary, while the $(10\bar{1}0)$ strains level off at a compressive value of about $-5 \times 10^{-4}$, the $(11\bar{2}0)$ strains increase rapidly, becoming zero after 6% compression and $+3 \times 10^{-4}$ after 8% deformation.

## Discussion

The basic premise of the discussion to follow is that all of the observed features of compressive deformation, texture evolution, residual strains and the shape of the stress-strain curve, can be interpreted in terms of the effects of deformation twinning. Our understanding of texture evolution and the workhardening behaviour are largely qualitative, based on a simple model of the initial rod texture. Interpretation of the evolution of residual strains is based on calculations made using the computer code QUEST [5,6], which calculates the thermo-mechanical behaviour of textured polycrystals from single crystal properties and which for this work has been modified to include deformation twinning.

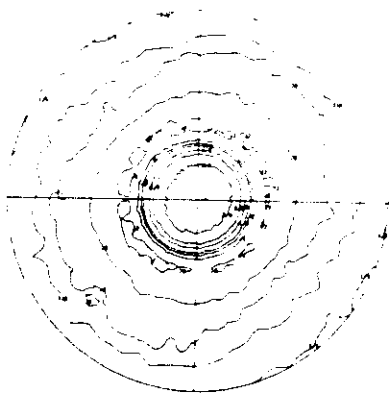

Figure 6(a)

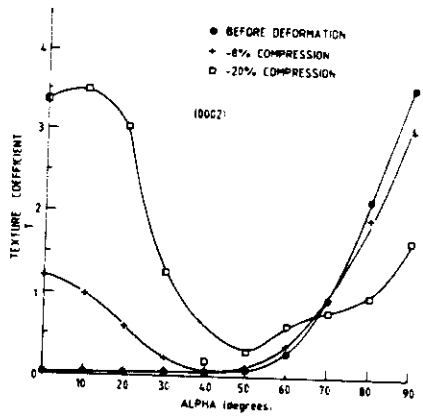


Figure 7(a)

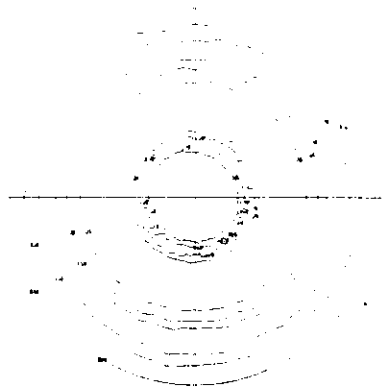

Figure 6(b)

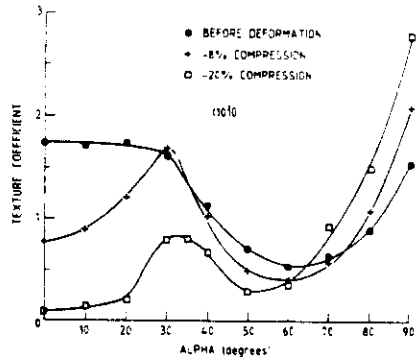


Figure 7(b)

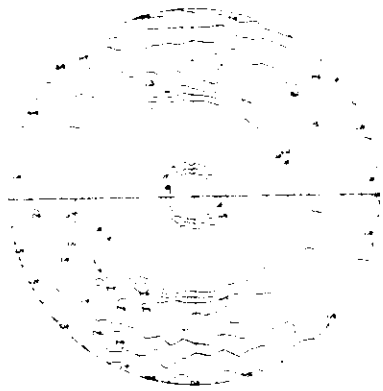

Figure 6(c)

Figure 6 - The (a) (0002), (b) (10$\bar{1}$0), and (c) (11$\bar{2}$0) pole figures after 20% compressive deformation.

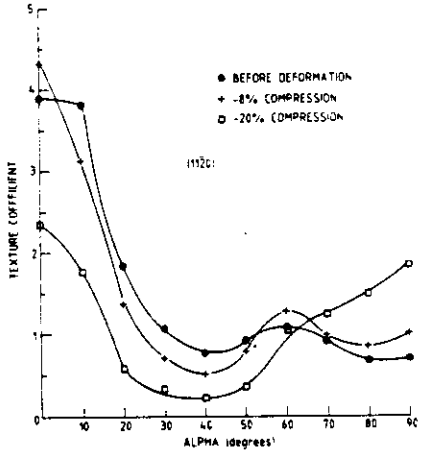


Figure 7(c)

Figure 7 - Dependence of the texture coefficient $T_c$ on the polar angle $\alpha$ and compressive deformation for the (a) (0002), (b) (10$\bar{1}$0) and (c) (11$\bar{2}$0) poles.

The simplified model of the texture considers two sets of grains. The basal plane normals of each set are distributed randomly in the RT ($\alpha$=90°) plane of the rod. Set #1 has a <2$\bar{1}\bar{1}$0> direction aligned with the rod axis while set #2 has <01$\bar{1}$0> aligned axially, as illustrated in Figure 11. In keeping with the relative intensities seen in the pole figures of Figure 2, set #1 is assigned a weight of 2/3, while that of set #2 is 1/3. Grains of set #1 have their (10$\bar{1}$0) poles oriented at $\alpha$ = 30° and 90° and their (11$\bar{2}$0) poles at $\alpha$ = 0° and 60°. The grains of set #2 are rotated by 30° about the <0002> direction relative to set #1 giving (10$\bar{1}$0) poles at 0° and 60°, and (11$\bar{2}$0) poles at 30° and 90°. The neutron diffraction experiments were done with the sample vertical and the scattering plane horizontal in the diffractometer. Consequently, each (hkil) diffraction line, in each (fixed-position) detector, arises from that unique subset of grains having the diffracting plane normal in the scattering plane, $\alpha$ = 90°, and bisecting the angle between the incident and diffracted beams of neutrons. Thus, only subsets from set #1 could give (10$\bar{1}$0) intensity and only subsets from set #2 could contribute to (11$\bar{2}$0) peaks (see Figure 11). The (0002)

intensity, on the other hand, would arise from the texture-weighted average of the (0002) interplanar spacings in both the #1 and #2 sets, since each have their <0002> directions in the scattering plane at $\alpha = 90°$. However, as discussed earlier, the axisymmetry of the texture, the deformation and the diffractometer dictate that the residual strains in the grains in each set will be identical (when expressed in crystal coordinates), although they need not be equal to each other. The most highly stressed twinning systems are the $(01\bar{1}2)\langle 0\bar{1}11\rangle$ and $(0\bar{1}12)\langle 01\bar{1}1\rangle$ in set #2; twinning on these systems produces an 85° rotation of the $\langle 01\bar{1}0\rangle$ pole about the $\langle 2\bar{1}\bar{1}0\rangle$ direction as shown in Figure 11. Thus the twinned volume contributes to the same $(11\bar{2}0)$ diffraction peak as the parent crystal, although with a much lower weighting factor at low strains.

## Texture Evolution

The net effect of twinning is to reorient the twinned volume by about 90° with respect to the parent grain, with the <0002> direction of the former replacing a $\langle 10\bar{1}0\rangle$ direction of the latter. Thus the changes in (0002) and $(10\bar{1}0)$ texture coefficients, at a given $\alpha$, should be inversely related; a decrease in one necessitates an increase in the other. Comparison of Figure 7a and 7b confirms the expected inverse relationship between the texture coefficients for (0002) and $(10\bar{1}0)$. One can examine the effect of twinning in more detail by considering the rotations produced by twinning in each set of grains. For strains up to 2.5% the changes in the (0002) and $(10\bar{1}0)$ texture coefficients are negligible, since twinning has not yet been initiated. The slight increase in the $(11\bar{2}0)$ texture coefficient at $\alpha = 0°$ after ~ 2.5% strain is consistent with the rotation expected from slip. In compression, the orientation of set #1 is stable and that of set #2 would rotate to align a $(11\bar{2}0)$ pole along the compression axis. The opposite rotation is observed during tensile deformation, as seen in Figure 9. Twinning on the most highly stressed system in set #2 would cause the following: (0002) intensity would increase at $\alpha = 0°$ and decrease at $\alpha = 90°$; $(10\bar{1}0)$ intensity would decrease at $\alpha = 0°$ and increase at $\alpha = 90°$, and the $(11\bar{2}0)$ intensity would increase, but only slightly, at $\alpha = 90°$. All of these features are observed in Figure 7. Twinning on the secondary systems in set #2 would cause $(10\bar{1}0)$ to decrease, and (0002) to increase, at $\alpha = 60°$ and $(11\bar{2}0)$ to decrease at $\alpha = 30°$. The effect is observed, however only after ~20% strain, in keeping with the necessity of building up sufficient stress in the grains to activate the secondary systems. Similarly, activation of twinning in set #1, which would decrease $(10\bar{1}0)$ and increase (0002) at $\alpha = 30°$, is not observed until ~20% strain.

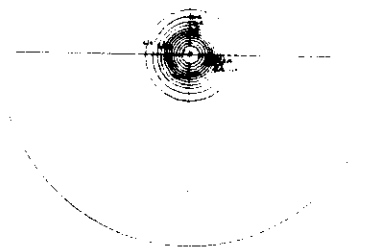

Figure 8 - The basal pole figure of Zircaloy-2 rod after 20% compression and a four-hour anneal at 925 K.

## Residual Stresses

The programme QUEST has been used previously [5-7] to model grain-interaction stresses in Zr alloys. It adopts the Taylor assumption, that the total strain given by the sum of the elastic, plastic and thermal components, is the same in every grain. Polycrystalline properties are

calculated from input defining texture, anisotropic elasticity and thermal expansion, and the single crystal yield surface, including the change in shape of the SCYS produced by workhardening by slip. Here we include the

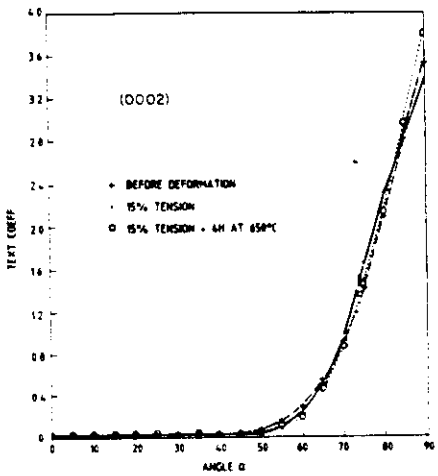


Figure 9(a)

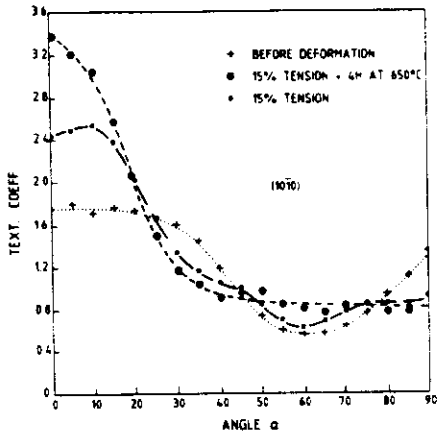


Figure 9(b)

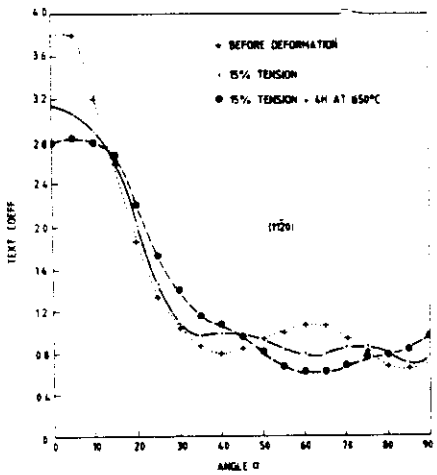


Figure 9(c)

Figure 9 - Dependence of $T_c$ on α and tensile deformation for the (a) (0002), (b) (10$\bar{1}$0), and (c) (11$\bar{2}$0) poles.

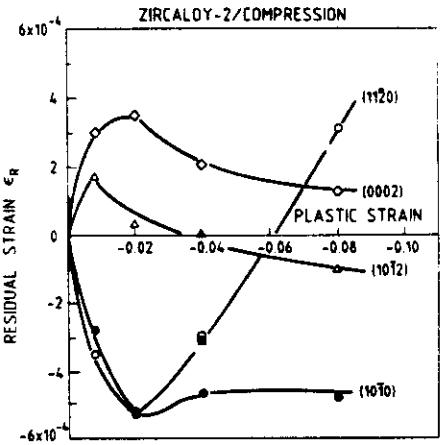


Figure 10 - Evolution of residual strains in compression measured normal to the (0002), (10$\bar{1}$2) and (10$\bar{1}$0) planes for grains with α=90°.

effects of deformation twinning. It is assumed, based on experimental evidence, that only tensile twins of the type (10$\bar{1}$2)<$\bar{1}$011> are active. These twins have a characteristic shear s = 0.167 [3]. We assume that twinning has an associated CRSS such that when the stress resolved in the (01$\bar{1}$2) plane in the <$\bar{1}$011> direction reaches a critical value, a fixed volume fraction of the grain, $V_t$, (taken to be 0.002) reorients by twinning. There is a unique relationship among the characteristic shear, the twinned volume and total shear strain produced by twin activity:

$\Delta\gamma^{TW}=V_t s$. The strain components in crystal coordinates are defined analogously to strains from slip by $\epsilon_i=m_i\Delta\gamma^{TW}$, where the m matrix is calculated from the coordinates of the twinning plane normal and shear direction. It is assumed that the activation of twinning is simultaneously accompanied by a relaxation of elastic strain by an amount equal in magnitude but opposite in sign to the plastic strain of the twin. Consequently, twins are considered only as a mechanism for stress relaxation and not for reorientation. The change in texture due to twinning has not yet been incorporated into the code. This assumption is valid for low strains where the total twinned volume is small.

Figure 12 plots the residual strains calculated by QUEST using a 10-grain model of the texture, with and without twinning, as a function of the compressive plastic strain in the sample. In accord with the condition used experimentally and discussed previously, the (0002) residual strain was calculated from the weighted average of the basal plane spacings in sets #1 and #2. The $(10\bar{1}0)$ and $(11\bar{2}0)$ residual strains originate from grains of set #1 and #2, respectively (see Figure 11). The elastic-plastic transition is completed, and the sample is fully plastic, after about 0.1% plastic strain. The evolution of residual strains during this interval results from the stress "vector" moving on the SCYS to the final vertex; the change in shape of the SCYS is negligible. The evolution of residual strains with further deformation is determined by the change in shape of the SCYS produced by workhardening. In the absence of twinning (enforced by setting the CRSS for twinning to an unrealistically high value) the basal and prism residual strains increase monotonically, but in the opposite sense to that observed (and calculated) for tensile deformation. With the twinning CRSS set to a realistic value [8], twinning begins on the $(01\bar{1}2)<0\bar{1}11>$ and $(0\bar{1}12)<01\bar{1}1>$ systems in the grains of set #2 after about 0.15% plastic deformation; the grains of set #1 do not twin until much higher strains. The relaxation of the (0002) and $(11\bar{2}0)$ residual strains is a consequence of the twinning in set #2; the grains of set #1 do not twin and the $(10\bar{1}0)$ residual strains are essentially unaltered. The twin shears of the systems activated in set #2 produce no component of strain normal to the twin shear plane and thus the $(2\bar{1}\bar{1}0)$ interplanar spacing is unaltered by the formation of a twin. The change in slope of the curve of $(11\bar{2}0)$ residual strain in Figure 12 is a consequence of the change in workhardening, and thus the rate of change of the shape of the SCYS. Without twinning, deformation occurs by prism and pyramidal slip; with twinning the imposed strain is accommodated by the twinning shear and prism slip. While the general relaxation of residual strains is in agreement with the data of Figure 10, several important features are not. The calculation of the evolution of residual strains with plastic deformation

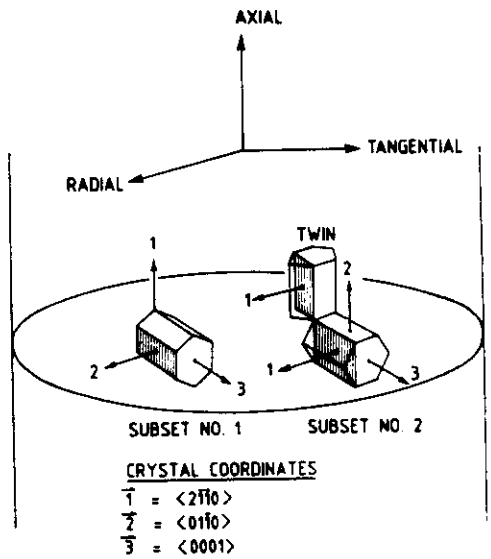


Figure 11 - Model describing the crystallographic texture of annealed Zircaloy-2 rod.

of the rod is much too rapid. This general feature of the QUEST code has been discussed previously [5,6] and is a consequence of the Taylor assumption. The relaxation of the (0002) and (10$\bar{1}$0) residual strains is less than observed experimentally and, most importantly, the calculated behaviour of the (11$\bar{2}$0) residual strain is not as observed experimentally. The stress relaxation calculated assuming that the twin shear is accommodated uniformly, elastically, by simple shear in the parent grain is insufficient to predict the observed behaviour, namely that the (11$\bar{2}$0) strains rapidly evolve from a compressive to a tensile state once twinning begins. The indisputable conclusion from the experimental results is that twinning must produce a strain relaxation in the direction normal to the shear plane. Such a strain could result if either the plastic strain of the twin itself is not as calculated from its shear alone, or if the accommodation of the twin strain is not unifom elastic shear within the parent grain. Accommodation modes for twins have been discussed by Reed-Hill [9], and will be considered in a future paper.

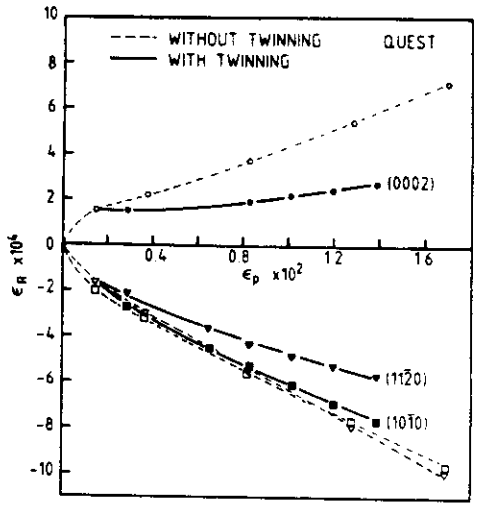


Figure 12 - Evolution of residual strains in compression normal to the (0002), (10$\bar{1}$0) and (11$\bar{2}$0) planes calculated by QUEST. Open symbols describe the evolution of $\epsilon_R$ without twinning, closed symbols that with twinning. The CRSS for prism glide was 115 MPa, for pyramidal glide, 230 MPa and for twinning, 290 MPa.

Stress-Strain Curve

The strength differential and the difference in the workhardening rate in tension and compression over the first few per cent deformation are a consequence of the residual stresses produced by differential thermal contraction during cooling from the annealing temperature [6]. The decrease in workhardening rate with increasing flow stress in tension is in accord with behaviour in other metals, so it is only the increase in workhardening rate during the first 20% compression that requires interpretation. The asymmetry of the SCYS is a consequence of the CRSS for pyramidal slip being much higher than that for prism slip. The twinned volume in a compressed rod is oriented with its <c> direction axially. Consequently, the resolved shear stress for prism slip is low and plastic deformation will occur primarily on the pyramidal systems. Thus, the effect of the reoriented volume will be to increase the flow stress and the apparent workhardening rate $d\sigma/d\epsilon$ would increase with increasing twinned volume, as observed experimentally. This suggestion is supported by recent experiments [10] which show that the tensile proportional limit in a compressed-and-recrystallized rod with the texture of Figure 8 is 350 MPa, an increase of 140 MPa over that in as-received rod.

## Conclusions

1. The evolution of texture during the compressive deformation of Zircaloy-2 rod is the result of deformation twinning on the $(10\bar{1}2)\langle\bar{1}011\rangle$ systems.

2. The increase in the apparent workhardening rate is the result of the increased flow stress of the twinned volume.

3. The observed relaxation of residual grain-interaction strains, and in particular the strain in the $\langle 11\bar{2}0\rangle$ direction, cannot be explained by the shear strain of the twin alone, suggesting that a relaxation strain, normal to the shear plane of the twin is significant in Zircaloy-2.


## Acknowledgements

This work has benefitted from the use of the Intense Pulsed Neutron Source at Argonne National Laboratory which is funded by the U.S. Department of Energy, BES-Materials Science, under Contract W-31-109-ENG-38".


## References


1. A. Akhtar, J. Nucl. Mater., 47 (1973) 19.

2. E. Tenckhoff, ASTM STP 551 (1974) 179.

3. R.G. Ballinger, "The Anisotropic Mechanical Behaviour of Zircaloy-2", Garland Publishing (1979).

4. S.R. MacEwen, J. Faber Jr. and A.P.L. Turner, Acta Metall., 31 (1983) 657.

5. S.R. MacEwen and C. Tome, 7th International Conference on "Zirconium in the Nuclear Industry", June 24-27, 1985, Strasbourg, France.

6. S.R. MacEwen, C. Tome and J. Faber Jr., to be published.

7. S.R. MacEwen, Proceedings of the International Workshop on Mechanisms of Irradiation Creep and Growth, June 22-25, 1987, Hecla Island, Manitoba, Canada.

8. C. Tome and U.F. Kocks, Acta Metall., 33 (1985) 603.

9. R.E. Reed-Hill, "Physical Metallurgy Principles", D. Van Nostrand Co., pg.629, 1973.

10. N. Christodoulou, unpublished work.